Possibilities of production of transfermium nuclei in charged-particle evaporation channels

Juhee Hong,[1] G. G. Adamian,[2] and N. V. Antonenko[2,3]
[1]*Rare Isotope Science Project, Institute for Basic Science, Daejeon 34047, Korea*
[2]*Joint Institute for Nuclear Research, Dubna 141980, Russia*
[3]*Mathematical Physics Department, Tomsk Polytechnic University, 634050 Tomsk, Russia*
(Received 30 July 2016; revised manuscript received 26 August 2016; published 11 October 2016)

The possibilities of direct production of the isotopes of transfermium nuclei ^{259,260}Md, ^{260,261}No, $^{261–264}$Lr, ^{264,265}Rf, $^{264–268}$Db, $^{266–269}$Sg, $^{266–271}$Bh, $^{267–274}$Hs, and $^{270–274}$Mt in various asymmetric hot fusion-evaporation reactions are studied. The excitation functions of the formation of these isotopes in the αxn and pxn evaporation channels are predicted for the first time. The optimal reaction partners and conditions for the synthesis of new isotopes are suggested. The products of the suggested reactions can fill a gap of unknown isotopes between the isotopes of heaviest nuclei obtained in the xn evaporation channels of the cold and hot complete fusion reactions.

DOI: 10.1103/PhysRevC.94.044606

I. INTRODUCTION

The hot actinide-based and cold ^{208}Pb- and ^{209}Bi-based complete fusion reactions have been intensively and successfully used to produce heavy and superheavy nuclei in the neutron-evaporation channels (xn channels) [1–15]. However, the synthesis of different isotopes of heaviest nuclei in these reaction channels is limited by the number of available stable projectiles and targets and the small production cross sections. There is a gap of unknown isotopes between the neutron-deficient superheavy nuclei obtained in cold fusion and the heaviest isotopes formed in hot fusion. Note that the α-decay chains of superheavy nuclei with the odd charge numbers synthesized in ^{48}Ca-induced fusion reactions end at this region of nuclides chart [1,2]. So, the direct production of some isotopes completing the α-decay chains might be interesting.

The multinucleon transfer reactions have been known for producing new isotopes for many years [16–22]. As demonstrated in Ref. [22], with asymmetry-exit-channel quasifission (multinucleon transfer) reactions ^{48}Ca + ^{238}U, ^{243}Am, and ^{244,246,248}Cm at energies near the corresponding Coulomb barriers one can produce new isotopes with the charge numbers $Z = 103$–108. However, new isotopes of heaviest nuclei can also be synthesized in the asymmetric actinide-based complete fusion-evaporation reactions with the emission of charged particles from the compound nucleus (CN). The production of the neutron-rich superheavy nuclei with charge numbers 112–117 in the proton evaporation channels is discussed already in Ref. [23]. The emission of charged particles competes with the neutron evaporation and fission. For the excited superheavy nucleus, the emission of charged particles is suppressed by the high Coulomb barrier. However, if after emission of charged particles the daughter nucleus has higher fission barrier than the parent nucleus, the survival probability can be relatively large and one can obtain new isotopes of transfermium nuclei with relatively large cross section. In addition, the complete fusion reactions have the larger experimental efficiency in the collection of products than the multinucleon transfer reactions and the choice of actinide targets in both types of reactions is a natural way to access the superheavy region.

The evaporation residue cross section [24–35]

$$\sigma_s(E_{\text{c.m.}}) = \sum_J \sigma_{\text{cap}}(E_{\text{c.m.}}, J) P_{\text{CN}}(E_{\text{c.m.}}, J) W_s(E_{\text{c.m.}}, J) \quad (1)$$

in the evaporation channel s depends on the partial capture cross section σ_{cap} for the transition of the colliding nuclei over the entrance (Coulomb) barrier, the probability of CN formation P_{CN} after the capture, and the survival probability W_s of the excited CN. In Eq. (1) the summation is over the orbital angular momenta J. In the first step of a fusion reaction the projectile is captured by the target. In the second step a formed dinuclear system (DNS) evolves into the CN in the mass asymmetry coordinate $\eta = (A_1 - A_2)/(A_1 + A_2)$ (A_1 and A_2 are the mass numbers of the DNS nuclei) [24–31,33,34]. Since the bombarding energy $E_{\text{c.m.}}$ of the projectile is usually higher than the Q value for the CN formation, the produced nucleus is excited. In the third step of the reaction the CN loses its excitation energy mainly by the emission of particles and γ quanta [36–43]. In the de-excitation of a CN, the charged-particle emission competes with the fission and neutron emission. The DNS model [24–26,33,34] used here is successful in describing fusion-evaporation reactions, especially related to the production of superheavy nuclei. Within the DNS model detailed calculations of excitation functions in different de-excitation channels of Th, U, Pu, Cm, and Hs, for which there are experimental data, have been performed in Refs. [32,33,35].

In the present article we focus on the possibility of the direct production of some unknown heaviest isotopes with $101 \leqslant Z \leqslant 109$ in the αxn and pxn evaporation channels with relatively high efficiency. We extend our model [35] to describe the production of nearby nuclei in the evaporation channels with emission of charged particles and neutrons in a consistent way. The de-excitation of the CN is treated with the statistical model using the level densities from the Fermi-gas model. We treat different asymmetric actinide-based complete fusion reactions. Our calculations are tested for several

TABLE I. The calculated evaporation residue cross sections $\sigma_{xn}^{\rm th}$ of the indicated xn evaporation channels in various reactions are compared with available experimental $\sigma_{xn}^{\rm exp}$.

Reaction	$E_{\rm c.m.}$ (MeV)	Channel	$\sigma_{xn}^{\rm th}$ (pb)	$\sigma_{xn}^{\rm exp}$ (pb)	Reference
^{12}C + ^{238}U → ^{250}Cf*	64.3	4*n*	5.8×10^7	6.2×10^7	[51]
	70.0	5*n*	8.9×10^7	1.0×10^8	
	79.5	6*n*	3.9×10^7	1.5×10^7	
	90.4	7*n*	1.9×10^6	3.0×10^6	
	109.5	8*n*	2.8×10^5	2.9×10^5	
^{12}C + ^{240}Pu → ^{252}Fm*	67.6	4*n*	2.2×10^6	1.3×10^6	[52]
^{16}O + ^{233}U → ^{249}Fm*	87.0	4*n*	4.9×10^4	2.0×10^5	[52]
	90.8	5*n*	4.1×10^3	1.3×10^4	
^{20}Ne + ^{232}Th → ^{252}Fm*	107.8	5*n*	2.1×10^4	$\sim(10 \pm 3) \times 10^3$	[53]
	111.4	6*n*	2.1×10^4	$\sim(6.0 \pm 2.5) \times 10^3$	
^{22}Ne + ^{232}Th → ^{254}Fm*	121.2	7*n*	1.3×10^4	$\sim(1.5 \pm 0.5) \times 10^4$	[53]
	129.4	8*n*	1.0×10^3	$\sim(3 \pm 1) \times 10^3$	
^{15}N + ^{248}Cm → ^{263}Lr*	76.4	4*n*	4.2×10^5	$\sim(1.3 \pm 0.2) \times 10^5$	[54]
	82.0	5*n*	7.6×10^5	$\sim(5.9 \pm 0.5) \times 10^5$	
^{27}Al + ^{232}Th → ^{259}Lr*	136.0	5*n*	2.3×10^3	$(1.7 \pm 0.5) \times 10^3$	[55]
	136.0	6*n*	1.8×10^3	$(1.3 \pm 0.5) \times 10^3$	
^{15}N + ^{249}Bk → ^{264}Rf*	75.5	4*n*	1.1×10^4	$(1.4 \pm 0.2) \times 10^4$	[56]
^{22}Ne + ^{242}Pu → ^{264}Rf*	104.9	4*n*	5.5×10^2	9.0×10^2	[57]
^{22}Ne + ^{244}Pu → ^{266}Rf*	104.9	4*n*	6.7×10^2	7.0×10^2	[58,59]
	104.9	5*n*	1.2×10^3	3.0×10^3	

known reactions [45–48] in which the excitation functions of actinides produced in the charged-particle evaporation channels have been measured.

In Secs. II–IV, we review the fusion model of Ref. [35] and extend the model for describing the charged-particle emission. In Sec. V, we compare the calculated excitation functions with available experimental data. For unknown isotopes of nuclei with $Z = 101$–109, we make predictions of the production cross sections of the charged-particle evaporation channels and indicate the optimal reactions for producing new isotopes. Finally, we summarize our results in Sec. VI.

II. EVAPORATION RESIDUE CROSS SECTION

Because the value of W_s strongly decreases with increasing angular momentum and $P_{\rm CN}$ weakly changes for relatively small angular momenta J, as in Ref. [35], we obtain from Eq. (1) the following approximate factorization:

$$\sigma_s(E_{\rm c.m.}) = \sigma_{\rm cap}^{\rm eff}(E_{\rm c.m.}) P_{\rm CN}(E_{\rm c.m.}) W_s(E_{\rm c.m.}), \qquad (2)$$

where $W_s(E_{\rm c.m.}) = W_s(E_{\rm c.m.}, J = 0)$ and $P_{\rm CN}(E_{\rm c.m.}) = P_{\rm CN}(E_{\rm c.m.}, J = 0)$ are the survival and fusion probabilities

TABLE II. The same as in Table I, but for other reactions.

Reaction	$E_{\rm c.m.}$ (MeV)	Channel	$\sigma_{xn}^{\rm th}$ (pb)	$\sigma_{xn}^{\rm exp}$ (pb)	Reference
^{18}O + ^{249}Bk → ^{267}Db*	86.7	4*n*	1.7×10^4	$(1.0 \pm 0.6) \times 10^4$	[60,61]
	92.3	5*n*	6.0×10^3	$(6.0 \pm 3.0) \times 10^3$	
^{19}F + ^{248}Cm → ^{267}Db*	95.8	5*n*	9.7×10^2	$(2.1 \pm 0.7) \times 10^3$	[60]
^{22}Ne + ^{241}Am → ^{263}Db*	108.1	4*n*	4.7×10^2	$(1.6 \pm 1.2) \times 10^3$	[62]
^{22}Ne + ^{243}Am → ^{265}Db*	106.4	4*n*	5.5×10^2	$(2.5 \pm 1.1) \times 10^2$	[63]
^{27}Al + ^{236}U → ^{263}Db*	138.2	5*n*	7.9×10^1	$(4.5 \pm 2.0) \times 10^2$	[64]
	146.3	6*n*	1.8×10^1	$(7.5 \pm 5.5) \times 10^1$	
^{31}P + ^{232}Th → ^{263}Db*	151.4	5*n*	5.0×10^1	$(1.2 \pm 1.0) \times 10^2$	[55]
^{18}O + ^{249}Cf → ^{267}Sg*	88.6	4*n*	7.1×10^2	$\sim 9 \times 10^2$	[65]
^{30}Si + ^{238}U → ^{268}Sg*	133.0	4*n*	1.1×10^1	$(1.0^{+1.0}_{-0.6}) \times 10^1$	[66]
	144.0	5*n*	2.6×10^1	$(6.7^{+6.7}_{-3.7}) \times 10^1$	
^{22}Ne + ^{249}Bk → ^{271}Bh*	113.0	4*n*	3.4×10^1	$(9.6^{+5.5}_{-2.5}) \times 10^1$	[59]
	113.0	5*n*	4.7×10^1	$25 - 250$	

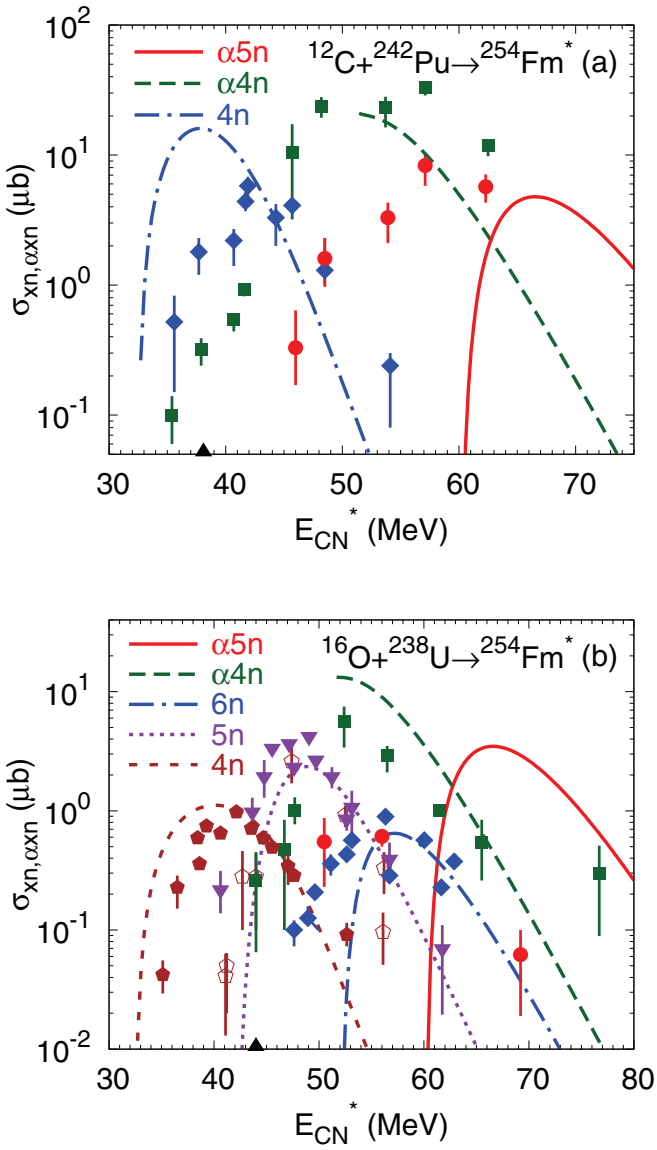

FIG. 1. The measured (symbols) and calculated (lines) excitation functions for αxn and xn evaporation channels. The mass table of Ref. [50] is used in the calculations. The black triangles at the energy axis indicate the excitation energy $E^*_{\rm CN} = V_b + Q$ of the CN. In the reaction $^{12}C + ^{242}Pu$ (a), the circles, squares, and diamonds represent the experimental data [45] with error bars for the $\alpha 5n$, $\alpha 4n$, and $4n$ evaporation channels, respectively. In the reaction $^{16}O + ^{238}U$ (b), the circles, squares, diamonds, inverse triangles, and pentagons represent the experimental data [45,67] with error bars for the $\alpha 5n$, $\alpha 4n$, $6n$, $5n$, and $4n$ channels, respectively.

reduced to zero angular momentum, respectively, and

$$\sigma_{\rm cap}^{\rm eff}(E_{\rm c.m.}) = \frac{\pi\hbar^2 J_{\rm max}^2}{2m\mu E_{\rm c.m.}}\left[1+\frac{\mu}{\zeta}\ln\{1+\exp[\alpha_0(V_b - E_{\rm c.m.})]\} - \frac{\mu}{\zeta}\ln\{1+\exp[\alpha_0(V_b - E_{\rm c.m.}) + \zeta/\mu]\}\right] \quad (3)$$

is the effective capture cross section for the transition of the colliding nuclei over the Coulomb barrier with the height V_b. Here, the maximum orbital angular momentum $J_{\rm max} = 10$, m is the nucleon mass, $\mu = A_1A_2/(A_1 + A_2)$ is the reduced mass number, and the energy barrier V_b is determined by the Coulomb barrier for the side-by-side orientation of deformed nuclei in the entrance channel. The parameters have been adjusted as $\alpha_0 = 0.5\,{\rm MeV}^{-1}$ and $\zeta = 41.47$ [35]. Usig Eq. (3), we have effectively taken the orientation effects into account to reproduce the available experimental data [35].

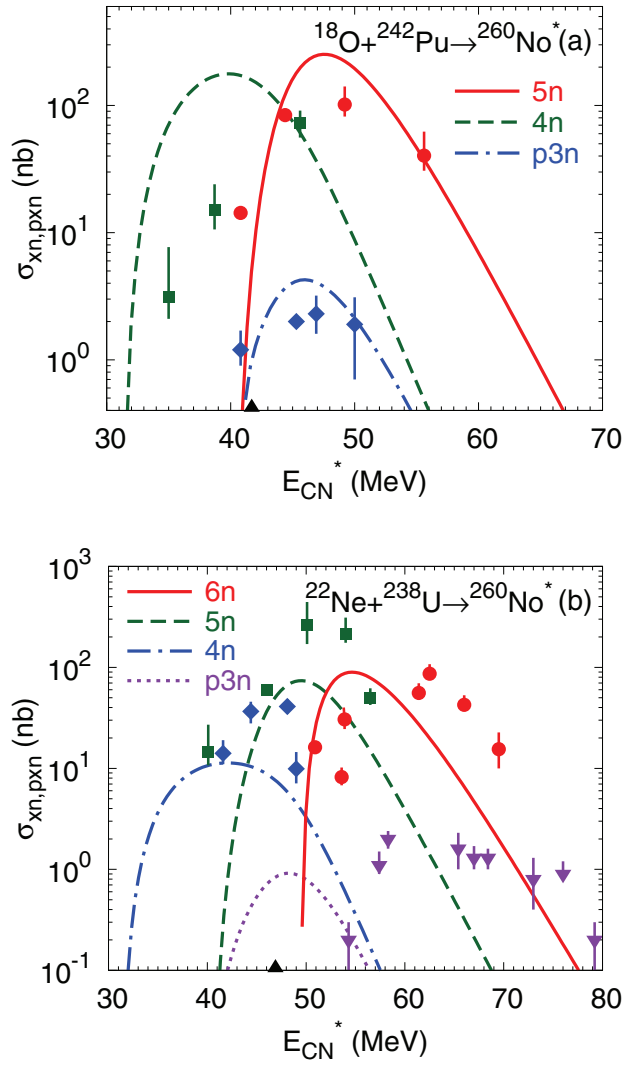

FIG. 2. The same as in Fig. 1, but for the reaction channels indicated. In the reaction $^{18}O + ^{242}Pu$ (a), the circles, squares, and diamonds represent the experimental data [46] with error bars for the $5n$, $4n$, and $p3n$ evaporation channels, respectively. In the reaction $^{22}Ne + ^{238}U$ (b), the circles, squares, diamonds, and inverse triangles represent the experimental data [46] with error bars for the $6n$, $5n$, $4n$, and $p3n$ channels, respectively.

III. PROBABILITY OF COMPLETE FUSION

After the colliding nuclei is captured in a dinuclear configuration by the pocket of the depth B_{qf}^R in the nucleus-nucleus potential, the relative kinetic energy is transferred into the potential and excitation energies. In the reactions considered the initially formed DNS is usually in the local potential minimum on the potential energy surface. The microscopical

effects are taken into account to calculate the potential energy in η. The DNS develops in time by diffusion in the mass asymmetry coordinate η and in the relative coordinate R. The fusion probability $P_{\rm CN}$ gives the probability that the DNS crosses the inner fusion barrier $B_\eta^{\rm fus}$ in η and forms the CN. The barrier B_{qf}^{η} in the driving potential is situated behind the initial mass fragmentation η_i toward smaller values of $|\eta| < |\eta_i|$ and hinders the DNS to proceed to more symmetric configurations. The DNS can decay in two ways, namely in R from the initial configuration or can first evolve to more symmetric configurations from which it decays in R with a larger probability because of the larger Coulomb repulsion. In order to calculate $P_{\rm CN}$, in Ref. [33] we suggested the approximate expression

$$P_{\rm CN} \approx \frac{1.25\exp\left[-\left(B_\eta^{\rm fus}-B_{qf}\right)/T_{\rm DNS}\right]}{1+1.25\exp\left[-\left(B_\eta^{\rm fus}-B_{qf}\right)/T_{\rm DNS}\right]}, \qquad (4)$$

where $B_{qf}=\min(B_{qf}^R,B_{qf}^\eta)$ and $T_{\rm DNS}=\sqrt{E^*_{\rm DNS}/a}$ is the temperature of the initial DNS ($a=A/10$ MeV^{-1} is the level density parameter and $E^*_{\rm DNS}$ is the excitation energy of the initial DNS). As follows from our calculations, Eq. (4) provides a good approximation of fusion probabilities obtained with the solution of the master equation in coordinates η and R. The height of the fusion barrier in η is strongly influenced by the shell and deformation effects because it is determined from the DNS potential energy,

$$U(R,\eta,\beta_i,J)=B_1+B_2+V(R,\eta,\beta_i,J), \qquad (5)$$

where the shell and deformation effects come from the binding energies B_i ($i=1,2$) of nuclei and nucleus-nucleus interaction potential V, and β_i ($i=1,2$) are the deformation parameters of the DNS nuclei in their ground states. The details of calculations of the barriers $B_\eta^{\rm fus}$ and B_{qf} and the temperature $T_{\rm DNS}$ are presented in Refs. [24–26].

IV. SURVIVAL PROBABILITY

Because σ_s is factorized into three factors in Eq. (2) with $W_s(E_{\rm c.m.},J=0)=W_s(E_{\rm c.m.})$ [32–34], the calculations of the survival probability are performed for $J=0$ only. The survival probability [36–43] under the evaporation of a certain sequence s of x particles is calculated as follows:

$$W_s(E^*_{\rm CN}) \approx P_s(E^*_{\rm CN})\prod_{i_s=1}^{x}\frac{\Gamma_{i_s}\left(E^*_{i_s}\right)}{\Gamma_t\left(E^*_{i_s}\right)}. \qquad (6)$$

Here, i_s, P_s, and $E^*_{i_s}$ are the index of the evaporation step, the probability of realization of the channel s at the initial excitation energy $E^*_{\rm CN}$ of the CN, and the mean values of excitation energy at step i_s, respectively. The total width Γ_t for the CN decay is the sum of the widths of particle evaporation Γ_i ($i=n,p,\alpha$ for neutron, proton, α particle, respectively) and fission Γ_f. The emissions of γ and other particles are assumed to be negligible to contribute to Γ_t.

In the case of emission of x neutrons ($s=xn$), the probability of realization of this evaporation sequence is [37]

$$P_{xn}(E^*_{\rm CN})=P[x]-P[x+1], \qquad (7)$$

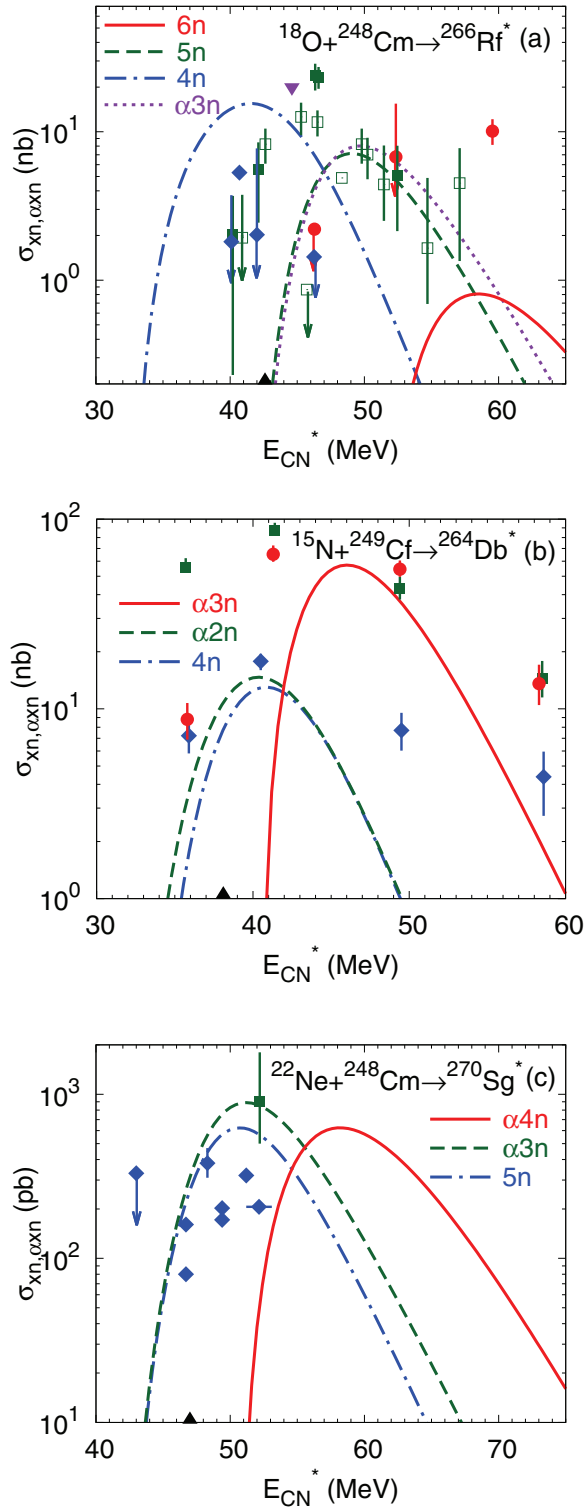

FIG. 3. The same as in Fig. 1, but for the reaction channels indicated. In the reaction ^{18}O + ^{248}Cm (a), the circles, squares, diamonds, and inverse triangle represent the experimental data [47,68] with error bars for the $6n$, $5n$, $4n$, and $\alpha 3n$ channels, respectively. In the reaction ^{15}N + ^{249}Cf (b), the circles, squares, and diamonds represent the experimental data [48] with error bars for the $\alpha 3n$, $\alpha 2n$, and $4n$ channels, respectively. In the reaction ^{22}Ne + ^{248}Cm (c), the square and diamonds represent the experimental data [69] with error bars for the $\alpha 3n$ and $5n$ channels, respectively.

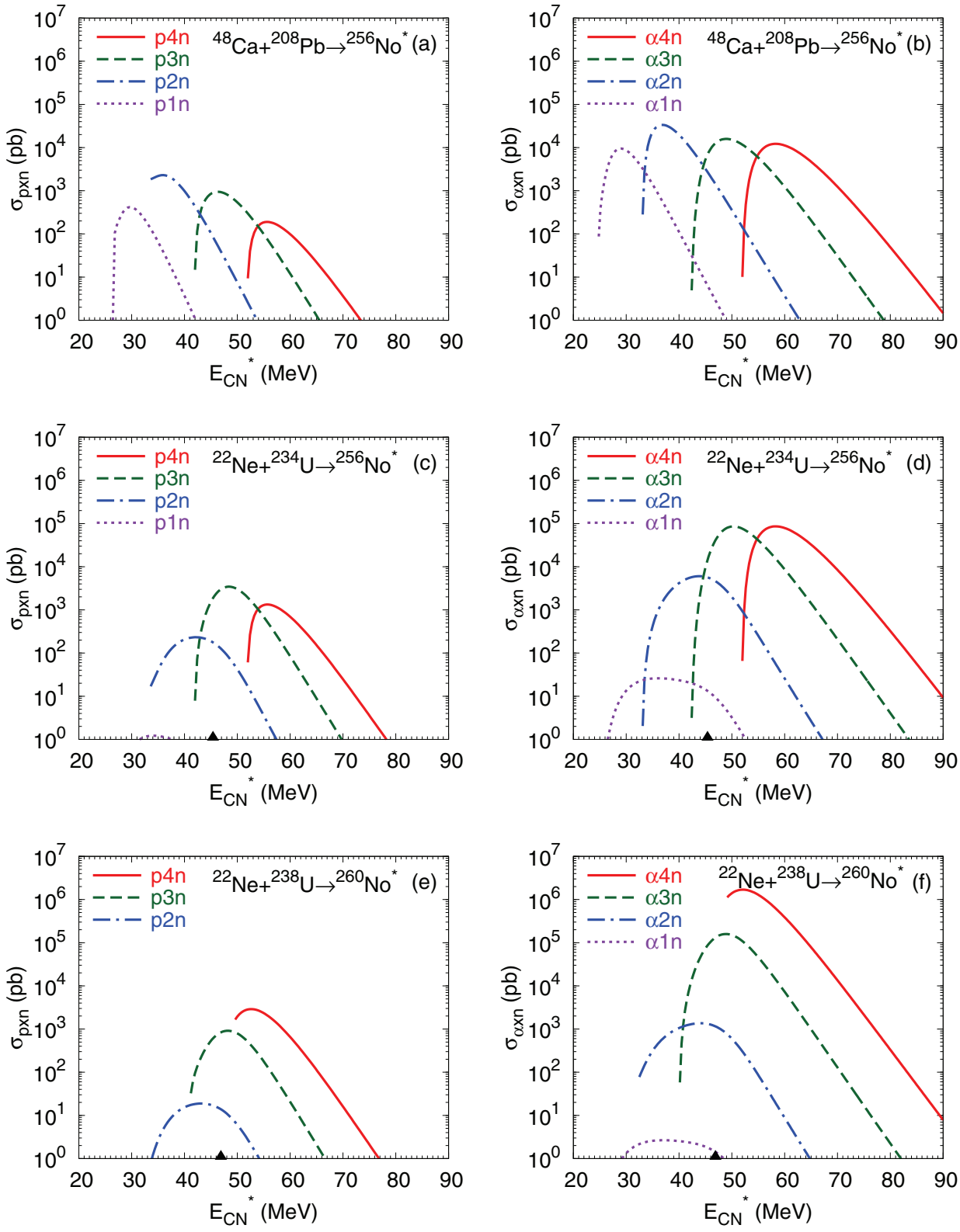

FIG. 4. The calculated excitation functions for the production of Fm and Md isotopes in the *pxn* and *αxn* evaporation channels of the reactions indicated. The mass table of Ref. [50] is used in the calculations.

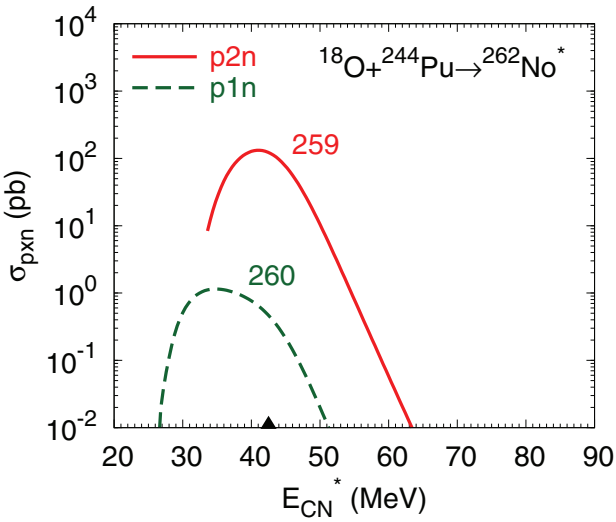

FIG. 5. The calculated excitation functions for the pxn evaporation channels in the reaction indicated. The mass numbers of the produced isotopes ^{259,260}Md are shown near the corresponding excitation functions. The black triangle at the energy axis indicates the excitation energy $E^*_{\rm CN} = V_b + Q$ of the CN. The mass table of Ref. [50] is used in the calculations.

where the function

$$P[x] = 1 - \exp(-\Delta_x/T)\left[1 + \sum_{i=1}^{2x-3} \frac{(\Delta_x/T)^i}{i!}\right] \quad (8)$$

defines the probability that at least x neutrons are evaporated at a given $E^*_{\rm CN}$. Here, $\Delta_x = E^*_{\rm CN} - \sum_{k=1}^{x} B_k$, where B_k is the separation energy of the evaporated neutron k, $T = \sqrt{E^*_{\rm CN}/(2a)}$ is the average temperature, which is taken as a constant during the whole evaporation process, and a is the level density parameter for the parent CN. The value of T in Eq. (8) is mainly responsible for the width of the excitation functions and does not much affect the maxima of the excitation functions. If the fission threshold B_f of the final residual nucleus after the emission of x neutrons is less than the neutron separation energy of that nucleus, B_{x+1} is replaced by B_f in the expression for Δ_{x+1} [37]. In order to calculate P_s for the channel with evaporation of charge particle i such as proton or α particle, we extend the formula for P_s by taking the Coulomb barrier V_j for the emission of this particle into account in the calculation of the value of binding energy B_k.

For the calculation of the Coulomb barrier, we use the expression

$$V_j = \frac{(Z - z_j)z_j e^2}{r_j\left[(A - m_j)^{1/3} + m_j^{1/3}\right]}, \quad (9)$$

where z_j (m_j) are the charge (mass) numbers of the charged particle (proton or α particle) and r_j is a constant. The charge Z (mass A) number corresponds to the CN. There are different theoretical estimations of r_j [36,43]. In the case of α emission, r_α varies from 1.3 to 1.78 fm. We obtain r_α from the energy of the DNS formed by the daughter nucleus and α particle. We calculate the Coulomb barrier in the interaction potential between the α particle and the daughter nucleus [49], and find the value of r_α from Eq. (9). For different nuclei considered, we obtained $r_\alpha = 1.5$–1.6 fm using this method. Thus, in the calculations of V_α we set $r_\alpha = 1.5$–1.6 fm for nuclei considered. The parameter r_p for the Coulomb barrier for proton emission is taken as $r_p = 1.7$ fm from Refs. [33,43]. As one can see, the values of σ_s near the maximum are almost insensitive to the variations of this parameter but far from the maximum they change up to one order of magnitude. We would like to stress the weak dependence of the calculated σ_s near the maxima of the excitation functions on the reasonable variation of all parameters discussed. Therefore, the results obtained in this paper have a small uncertainty near the maxima of the excitation functions which are important for the maximum yield of a certain nucleus. We estimate this uncertainty within a factor of 2–4.

With the level densities of the Fermi-gas model, the ratio of the emission width of a particle i ($i = n, p, \alpha$) to the fission width is [37]

$$\frac{\Gamma_i}{\Gamma_f} = \frac{4A^{2/3}a_f[E^*_{\rm CN} - B_i]}{ka_i\{2\sqrt{a_f[E^*_{\rm CN} - B_f(E^*_{\rm CN})]} - 1\}} \times \exp\{2\sqrt{a_i(E^*_{\rm CN} - B_i)} - 2\sqrt{a_f[E^*_{\rm CN} - B_f(E^*_{\rm CN})]}\}, \quad (10)$$

where $k = 9.8$ MeV and a_i is the level density parameter for the particle i evaporation channel. With $a_n = a$, the level density parameters for fission, proton emission, and α-emission channels are taken as $a_f = 1.04a$, $a_p = 0.96a$, and $a_\alpha = 1.15a$, respectively.

The fission barrier B_f has the liquid-drop $B_f^{\rm LD}$ [44] and microscopic $B_f^M(E^*_{\rm CN})$ parts: $B_f(E^*_{\rm CN}) = B_f^{\rm LD} + B_f^M(E^*_{\rm CN})$. For the considered isotopes of nuclei with $Z = 98$–109, $B_f^{\rm LD}$ is in the energy range of 0–4.4 MeV. The value $B_f^M = \delta W_{sd} - \delta W_{gr}$ is the difference between the shell correction δW_{sd} of nucleus at the saddle point and the shell correction δW_{gr} of nucleus in the ground state. Usually, one neglects the shell correction at the saddle point, $\delta W_{sd} \approx 0$ and, thus, $B_f^M = |\delta W_{gr}|$. Due to the dependence of the shell effects on the nuclear excitation, the value of B_f effectively depends on $E^*_{\rm CN}$ as

$$B_f(E^*_{\rm CN}) = B_f^{\rm LD} + B_f(E^*_{\rm CN} = 0)\exp[-E^*_{\rm CN}/E_d],$$

where the damping factor is $E_d = 25$ MeV. The pairing corrections $\Delta = 22/\sqrt{A}$, $11/\sqrt{A}$, and 0 for even-even, even-odd, and odd-odd nuclei, respectively, are regarded as follows: $E^*_{\rm CN} - B_j \rightarrow E^*_{\rm CN} - B_j - \Delta$, where $j = n, p, \alpha, f$, in Eq. (10). The neutron binding energies B_n and the microscopic corrections δW_{gr}^{mc} are taken from Ref. [50]. In order to avoid a double counting of pairing in the fission barrier which is purely the shell correction, $B_f^M = |\delta W_{gr}| = |\delta W_{gr}^{mc}| - \Delta$.

V. CALCULATED RESULTS

A. Comparison with experimental data

The fusion model discussed in Sec. II has been used to calculate the excitation functions and compare them with available experimental data in various reactions. In Tables I

and II, the experimental maximum cross sections of the xn evaporation channels are compared with the calculated evaporation residue cross sections. The disagreements up to a factor of ∼4 in some cases should be considered in light of the experimental uncertainties and the absence of a special fit in the parameters used.

Figs. 1–3 show the comparison between the measured and calculated excitation functions for the charged particle evaporation channels. For the reactions $^{12}C + ^{242}Pu \rightarrow ^{254}Fm^*$ and $^{16}O + ^{238}U \rightarrow ^{254}Fm^*$, there is no fusion hindrance, $P_{CN} \approx 1$. The survival probabilities are equal in both reactions for given channel. However, the $^{12}C + ^{242}Pu$ reaction has the lower $V_b + Q$ (indicated by the triangle on the energy axis), and the effective capture cross section is larger. As a result, the evaporation residue cross section is larger in the reaction $^{12}C + ^{242}Pu$. Although the measured cross sections of the $\alpha 5n$ channel are shifted to lower energies in Fig. 1(a), the maximum value of the experimental cross section agrees with the calculated result within the experimental and calculation uncertainties. In Fig. 1(b), the ratios between the measured (closed symbols [67]) cross sections of different xn channels are well reproduced with the DNS model. After emitting α particle and neutrons, the daughter nuclei have higher fission barriers (with larger B_f^{LD} at least) than the daughter nuclei in the neutron evaporation channel. The ratio of the maximum survival probabilities is $W_{\alpha xn}/W_{(x+1)n} \approx 10$ ($x = 4,5$) that is reflected on the calculated excitation functions. However, the experimental cross sections of the $\alpha 5n$ channel [45] are similar to those of the $6n$ channel [67] in the experiment where the $4n$ (open pentagons [45]) and $\alpha 5n$ channels are shifted to higher and lower energies, respectively. The excitation functions of neighboring channels might be overlapped. In the same experiments the radioactive α decays from the quasiparticle isomeric states could be mixed up with α-particle emissions. One can probably explain some of the existing discrepancies by such an effect.

The reactions $^{18}O + ^{242}Pu$ and $^{22}Ne + ^{238}U$ also lead to the same CN $^{260}No^*$. In comparison with the $^{22}Ne + ^{238}U$ reaction,

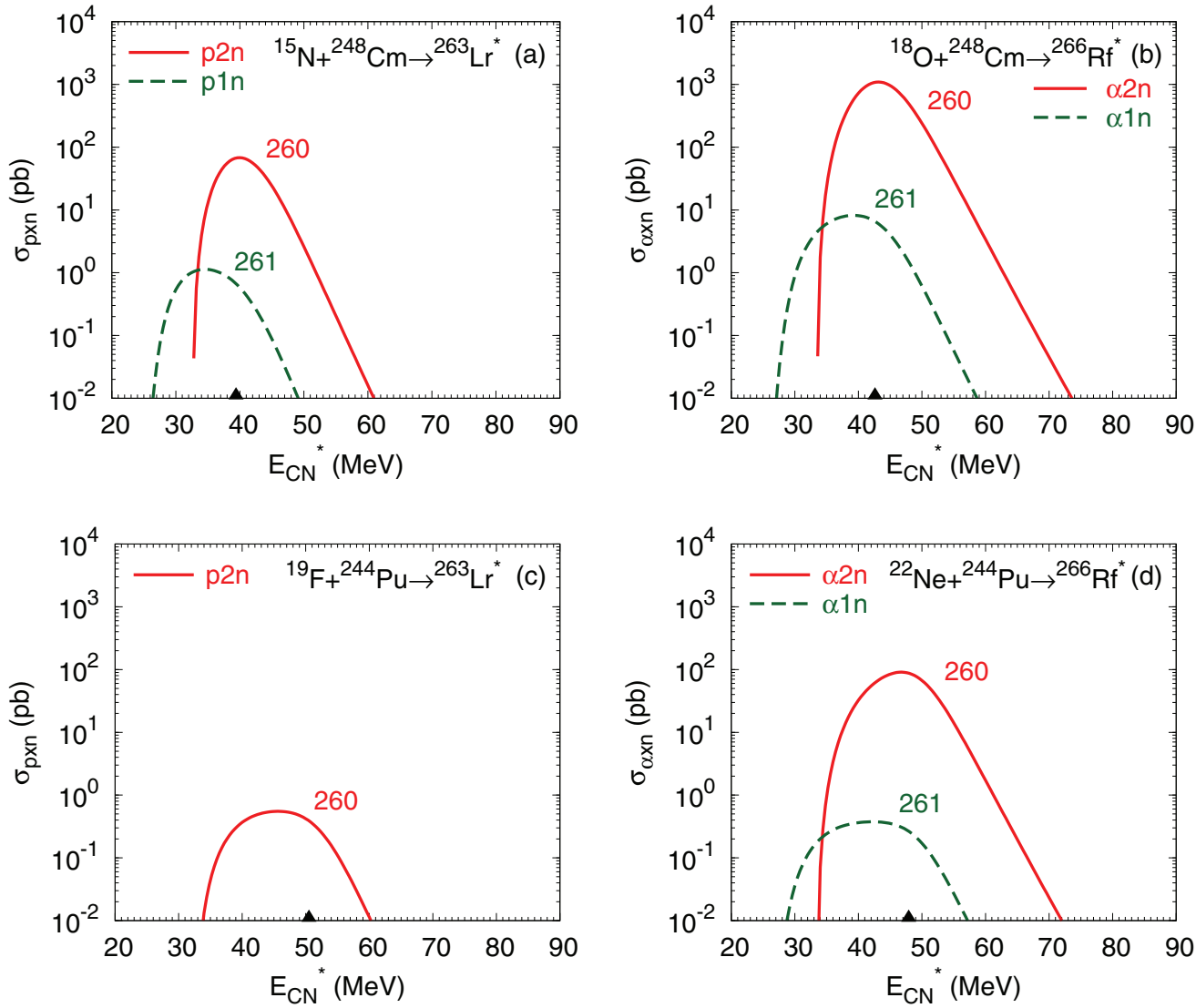

FIG. 6. The same as in Fig. 5, but for the production of isotopes ^{260,261}No in the pxn and αxn evaporation channels.

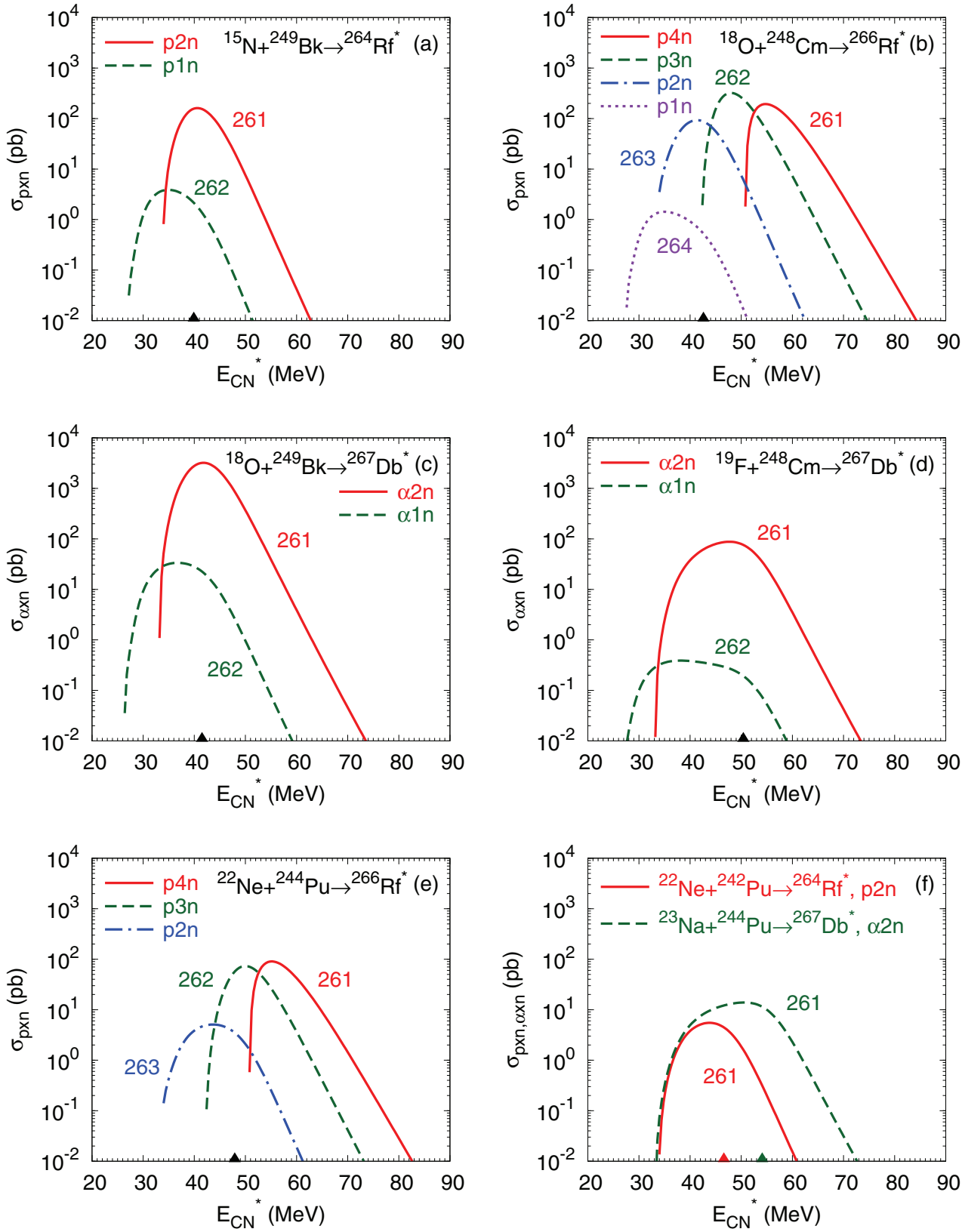

FIG. 7. The same as in Fig. 5, but for the production of isotopes $^{261-264}$Lr in the pxn and αxn evaporation channels of the reactions indicated.

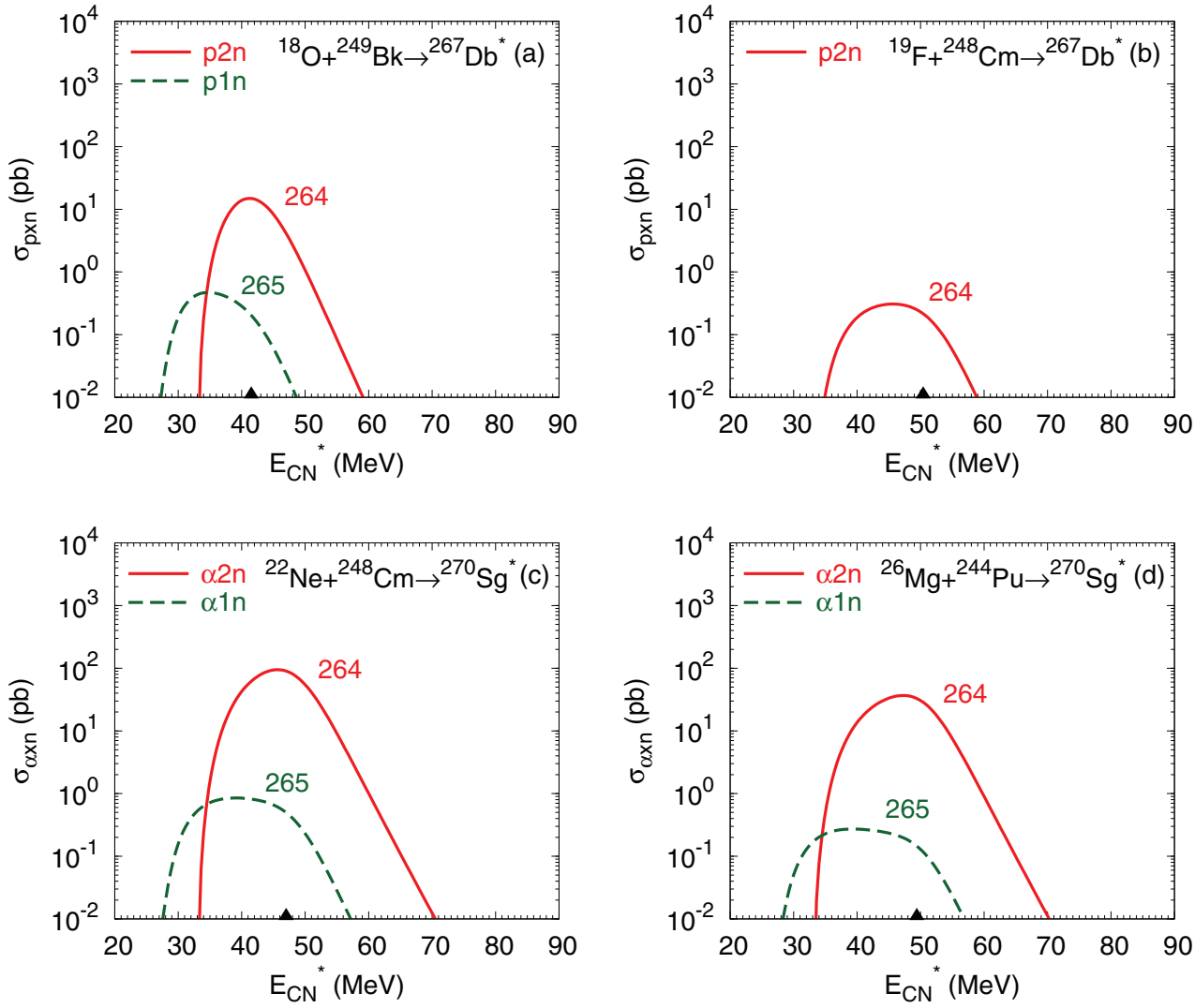

FIG. 8. The calculated excitation functions in the pxn and αxn evaporation channels of the reactions indicated. The mass numbers of the produced isotopes ^{264,265}Rf are shown near the corresponding excitation functions. The mass table of Ref. [50] is used in the calculations. The triangle at the energy axis indicates the excitation energy $E^{*}_{\rm CN} = V_b + Q$ of the CN.

the ^{18}O + ^{242}Pu reaction has the larger effective capture cross section and fusion probability. Consequently, the calculated evaporation residue cross sections are larger in the last reaction (Fig. 2).

In the proton-emission channels, the evaporation residue cross sections are usually smaller than those in the neutron evaporation channels (Fig. 2). This is because of the larger proton binding plus the Coulomb barrier energy ($B_p > B_n$) and the smaller level density parameter ($a_p < a_n$) (even though the daughter nuclei might have higher fission barriers). For the ^{18}O + ^{242}Pu (^{22}Ne + ^{238}U) reaction (Fig. 2), the maximum survival probability of the $p3n$ evaporation channel is about 10^3 times smaller than that of the $4n$ emission channel. Because in both reactions the $4n$-channel peak is under the Coulomb barrier V_b, the ratios of the maximum cross sections are $\sigma^{\rm th}_{4n}/\sigma^{\rm th}_{p3n} \approx 42$ and $\sigma^{\rm th}_{4n}/\sigma^{\rm th}_{p3n} \approx 12$ in the reactions ^{18}O + ^{242}Pu and ^{22}Ne + ^{238}U, respectively. These ratios agree with the experimental data within a factor of 2: $\sigma^{\rm exp}_{4n}/\sigma^{\rm exp}_{p3n}(^{18}{\rm O} + ^{242}{\rm Pu}) \approx 32$ and $\sigma^{\rm exp}_{4n}/\sigma^{\rm exp}_{p3n}(^{22}{\rm Ne} + ^{238}{\rm U}) \approx 21$. However, the experimental data in Fig. 2(b) are shifted to higher energies, especially for the $p3n$ evaporation channel. In the ^{22}Ne + ^{238}U (^{18}O + ^{242}Pu) reaction, the other ratios, $\sigma^{\rm th}_{5n}/\sigma^{\rm th}_{p3n} \approx 81$ ($\sigma^{\rm th}_{5n}/\sigma^{\rm th}_{p3n} \approx 59$) and $\sigma^{\rm th}_{6n}/\sigma^{\rm th}_{p3n} \approx 98$, are also close to the experimental ones, $\sigma^{\rm exp}_{5n}/\sigma^{\rm exp}_{p3n} \approx 132$ ($\sigma^{\rm exp}_{5n}/\sigma^{\rm exp}_{p3n} \approx 44$) and $\sigma^{\rm exp}_{6n}/\sigma^{\rm exp}_{p3n} \approx 43$, respectively.

As seen in Fig. 1(b), the formation of Cf isotopes is also possible in the (HI,αxn) reactions with higher survival probabilities and accordingly larger evaporation residue cross sections than those for the [HI,$(x+1)n$] reactions ($x = 4,5$). Similarly, in the ^{15}N + ^{249}Cf reaction the calculated excitation function for the $\alpha 3n$ evaporation channel is higher than one for the $4n$ emission channel [Fig. 3(b)]. For this reaction, the calculated cross-section ratio $\sigma^{\rm th}_{\alpha 3n}/\sigma^{\rm th}_{4n} \approx 4.4$ is quite close to the experimental one $\sigma^{\rm exp}_{\alpha 3n}/\sigma^{\rm exp}_{4n} \approx 3.7$ [48]. In the reactions ^{18}O + ^{248}Cm [Fig. 3(a)] and ^{22}Ne + ^{248}Cm [Fig. 3(c)], $\sigma_{\alpha xn} < \sigma_{(x+1)n}$. Although the measured ^{18}O + ^{248}Cm reaction data are

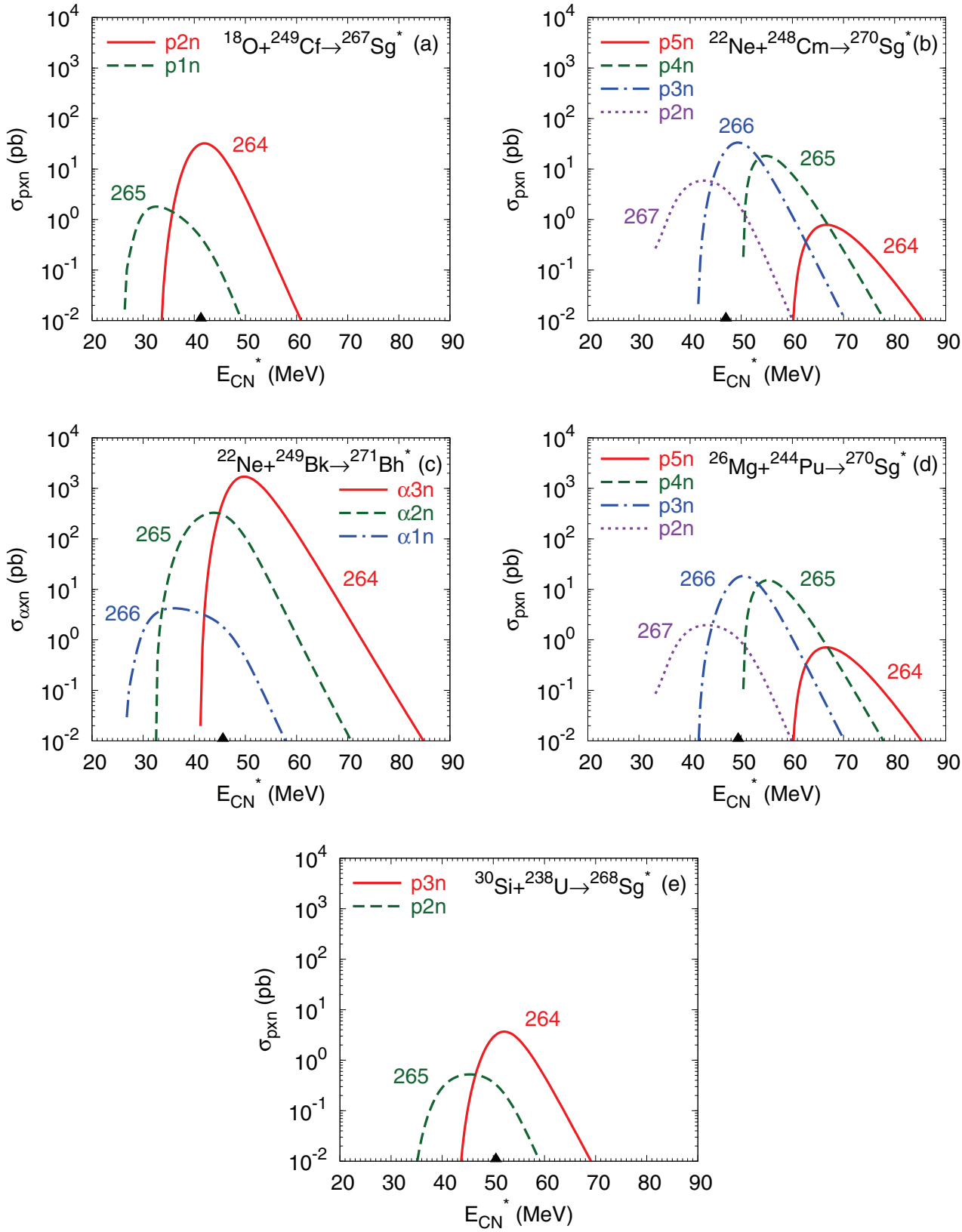

FIG. 9. The same as in Fig. 8, but for the production of the isotopes $^{264-267}$Db in the reactions indicated.

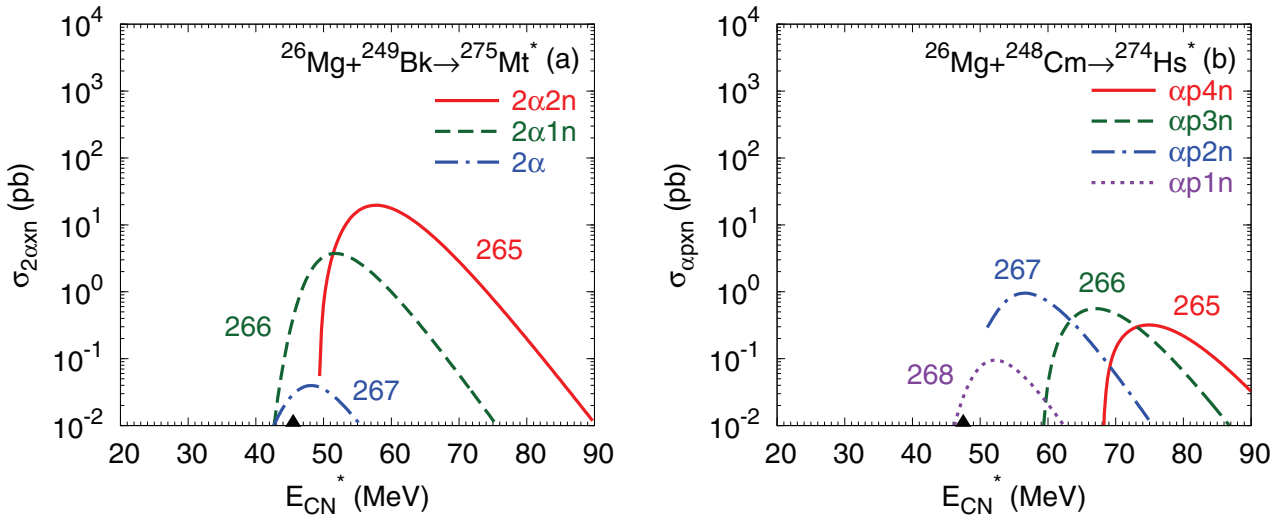

FIG. 10. The calculated excitation functions of the isotopes $^{265-268}$Db in the $2\alpha xn$ and αpxn evaporation channels. The reactions are indicated. The mass table of Ref. [50] is used in the calculations.

shifted to lower energies, the experimental $\sigma^{\rm th}_{\alpha 3n}/\sigma^{\rm th}_{5n} \approx 1.1$ and theoretical $\sigma^{\rm exp}_{\alpha 3n}/\sigma^{\rm exp}_{5n} \approx 1.6$ cross-section ratios are in good agreement. The calculated maximum cross section of the $4n$ evaporation channel is about twice as large as the measured one that is within the experimental uncertainties. The measured cross sections of the $6n$ emission channel are shifted to lower energies, and they are about an order of magnitude larger than the calculated ones. Note that in the ^{18}O + ^{248}Cm reaction the experimental uncertainties are large; the data points with arrow show the upper limit of the cross section [47,68].

B. Production of ^{259,260}Md

In asymmetric reactions ^{22}Ne + ^{234,238}U, $P_{\rm CN} \approx 1$. In the ^{48}Ca + ^{208}Pb reaction, the internal fusion and the quasifission barriers are almost equal to each other, and, thus, $P_{\rm CN} \approx 0.5$. Therefore, in these reactions the value of cross section is mainly determined by the survival probability of the pxn or αxn evaporation channel (Fig. 4). Because $\sigma^{\rm eff}_{\rm cap}(^{22}{\rm Ne} + ^{234}{\rm U}) > \sigma^{\rm eff}_{\rm cap}(^{48}{\rm Ca} + ^{208}{\rm Pb})$ and $P_{\rm CN}(^{22}{\rm Ne} + ^{234}{\rm U}) > P_{\rm CN}(^{48}{\rm Ca} + ^{208}{\rm Pb})$ at energies above the corresponding Coulomb barriers, the production cross sections of isotopes $^{248-251}$Fm and $^{251-254}$Md in the ^{22}Ne + ^{234}U reaction are larger than those in the ^{48}Ca + ^{208}Pb reaction.

The isotopes ^{259,260}Md can be produced in the pxn channels of the ^{18}O + ^{244}Pu reaction (see Fig. 5) where $P_{\rm CN} \approx 1$ and the evaporation residue cross section depends only on the survival probability and the effective capture cross section. The survival probability of the $p2n$ channel is smaller than one of the pn channel. At energies under the Coulomb barrier V_b, the effective capture cross section increases with the CN excitation energy [35]. Because the pn-channel peak is under the barrier, the calculated cross sections of the ^{260}Md isotope are smaller than those of the ^{259}Md isotope.

C. Production of ^{260,261}No

The isotopes ^{260,261}No (^{261}No is still unknown) can be produced in the pxn and αxn evaporation channels of the complete fusion reactions ^{15}N + ^{248}Cm → ^{263}Lr* [Fig. 6(a)], ^{19}F + ^{244}Pu → ^{263}Lr* [Fig. 6(c)] and ^{18}O + ^{248}Cm → ^{266}Rf* [Fig. 6(b)], ^{22}Ne + ^{244}Pu → ^{266}Rf* [Fig. 6(d)]. In these very asymmetric reactions, the fusion probability is almost equal to 1. Since in the ^{15}N + ^{248}Cm (^{18}O + ^{248}Cm) reaction the value of $E^{*}_{\rm CN} = V_b + Q$ is smaller by about 11 MeV (6 MeV) than one in the ^{19}F + ^{244}Pu (^{22}Ne + ^{244}Pu) reaction leading to the same CN, the effective capture cross section is larger in the former reaction. Thus, the maximum evaporation residue cross section of the pxn channel (αxn channel) in the ^{15}N + ^{248}Cm (^{18}O + ^{248}Cm) reaction is about two orders (one order) of magnitude larger.

Among various reactions considered above, the ^{18}O + ^{248}Cm reaction seems to be the most suitable for the synthesis of new isotopes ^{260}No and ^{261}No with the maximum cross sections $\sigma_{\alpha 2n} = 1$ nb and $\sigma_{\alpha 1n} = 10$ pb, respectively.

D. Production of $^{261-264}$Lr

The excitation functions for the αxn and pxn evaporation channels are presented in Fig. 7. Although the fusion ($P_{\rm CN} \approx 1$) and the survival probabilities are almost equal in the reactions ^{18}O + ^{249}Bk, ^{19}F + ^{248}Cm, and ^{23}Na + ^{244}Pu, the evaporation residue cross sections of the αxn evaporation channels are different in Figs. 7(c), 7(d), and 7(f) due to the differences in the capture cross sections (different values of V_b and Q). The evaporation residue cross section in the ^{18}O + ^{249}Bk reaction is the largest one: The production cross sections of the isotopes ^{261}Lr and ^{262}Lr in the $\alpha 2n$ and αn channels are expected with the cross sections 3 nb and 30 pb, respectively. In the reactions ^{15}N + ^{249}Bk [Fig. 7(a)], ^{18}O + ^{248}Cm [Fig. 7(b)], and ^{22}Ne + ^{242,244}Pu [Figs. 7(f) and 7(e)], the main discrepancies appear to be attributable

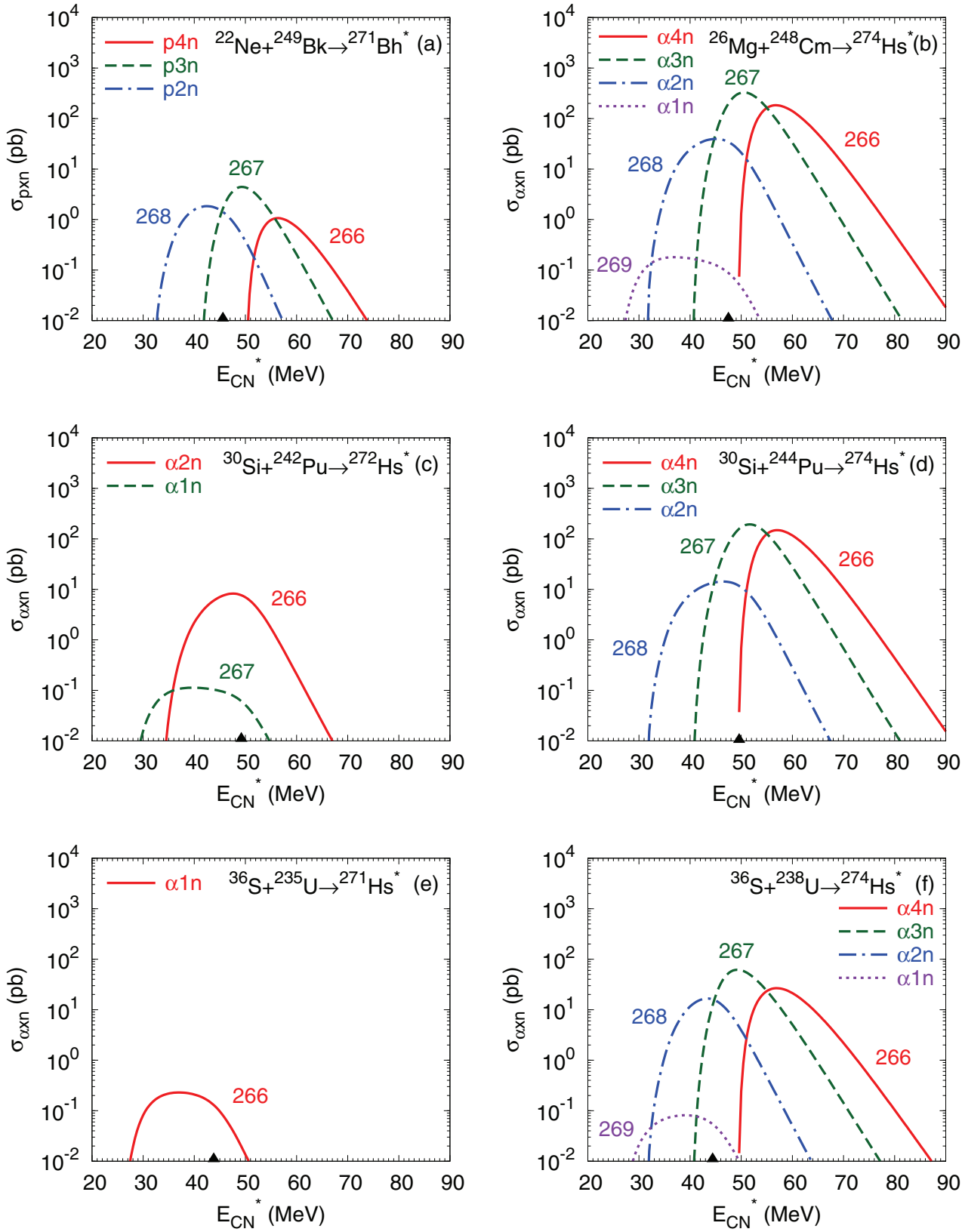

FIG. 11. The same as in Fig. 8, but for the production of the isotopes $^{266-269}$Sg in the reactions indicated.

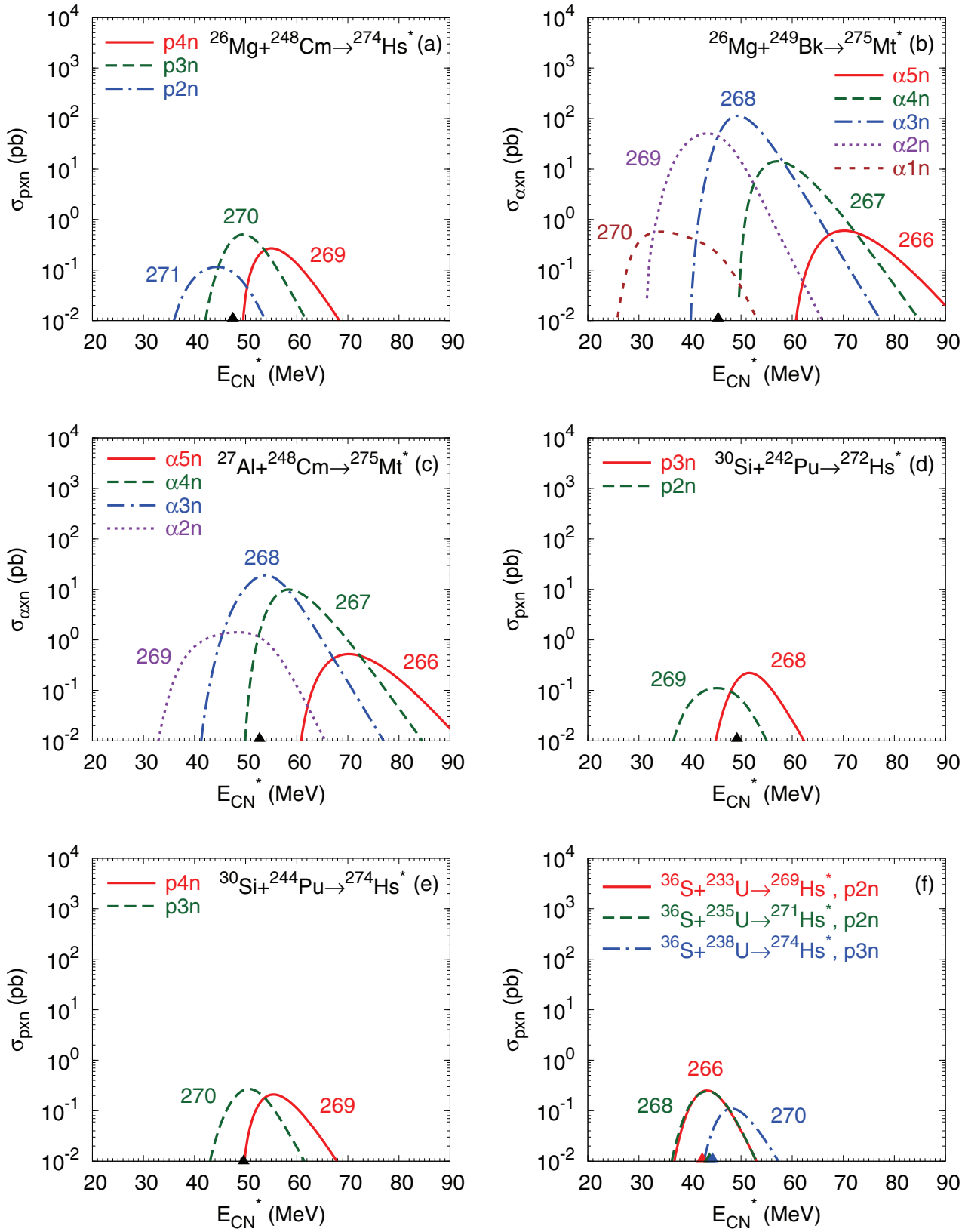

FIG. 12. The same as in Fig. 8, but for the production of the isotopes $^{266–271}$Bh in the reactions indicated.

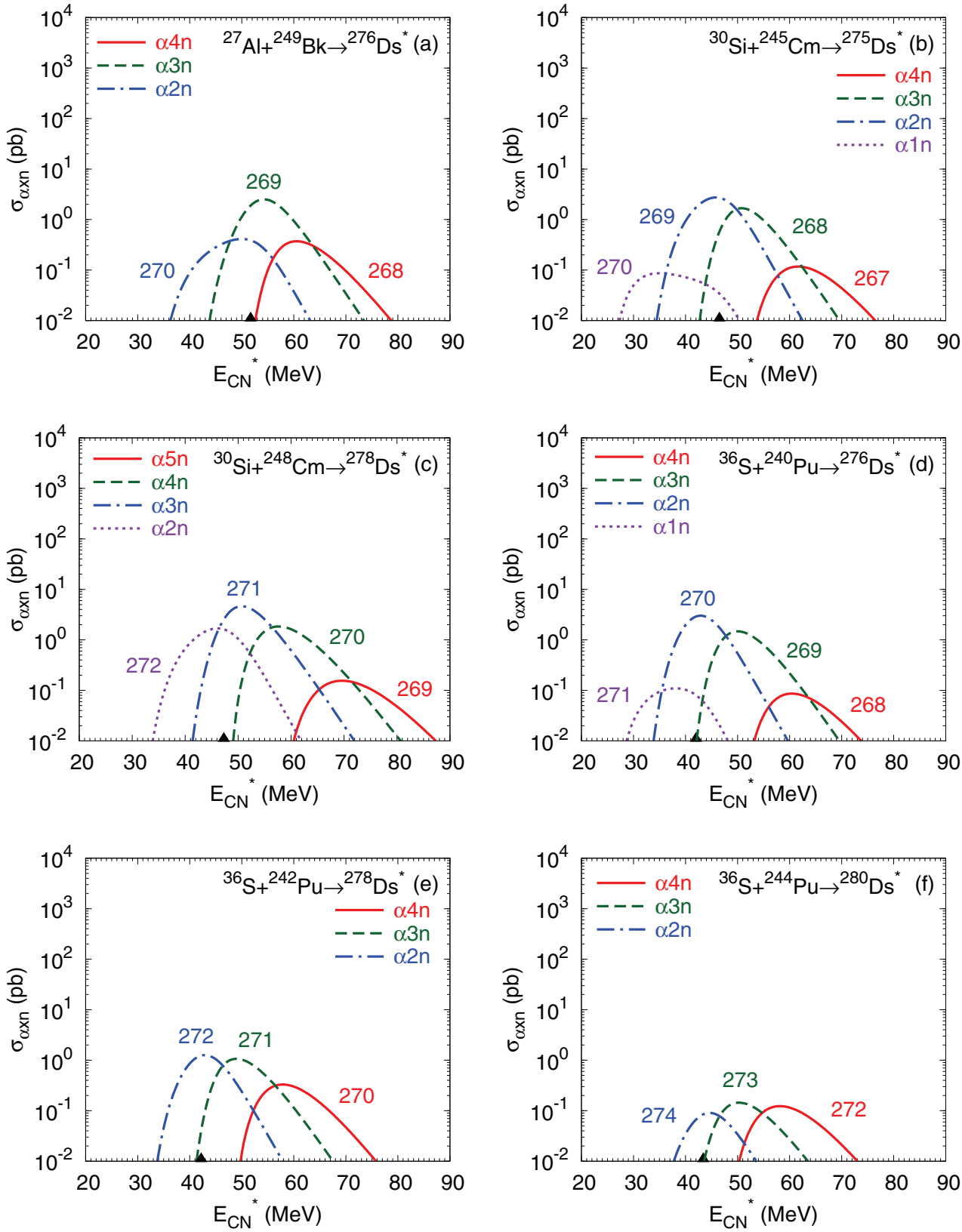

FIG. 13. The same as in Fig. 8, but for the production of the isotopes $^{267-274}$Hs in the αxn evaporation channels of the reactions indicated.

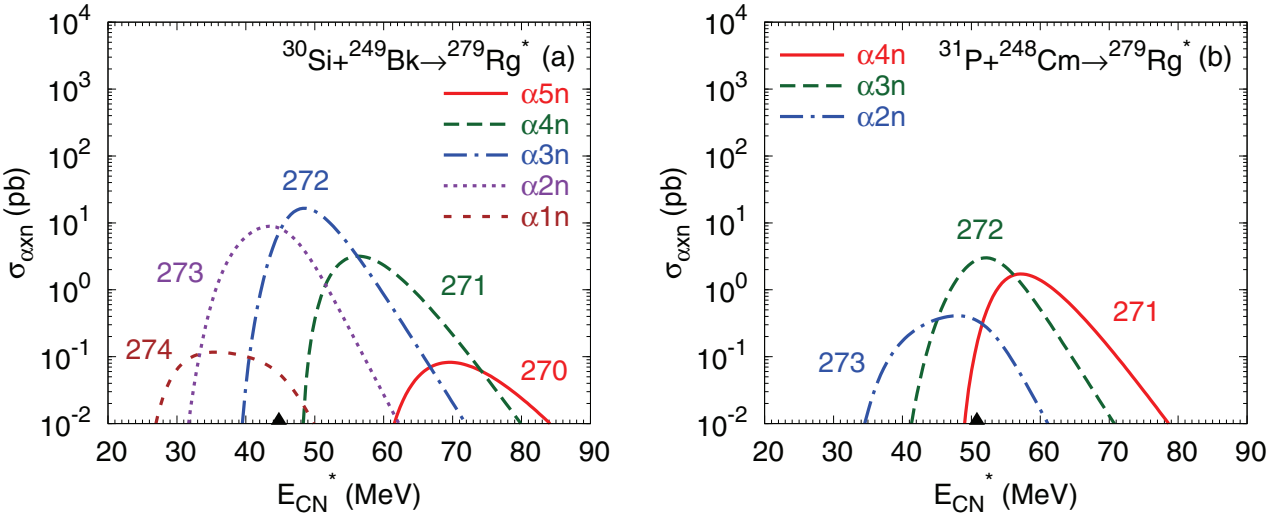

FIG. 14. The same as in Fig. 8, but for the production of the isotopes $^{270–274}$Mt in the αxn evaporation channels of the reactions indicated.

to the difference of their capture cross sections. For the production of unknown isotopes ^{263,264}Lr in the pxn evaporation channels, the $^{18}O+^{248}Cm$ reaction is the best one. The cross sections of the isotopes ^{262,263,264}Lr are expected to be about of 300, 90, and 1.4 pb, respectively. We expect that the production of ^{261}Lr isotope is the most favorable in the $^{18}O+^{249}Bk$ reaction with emission of the α particle from the CN.

E. Production of ^{264,265}Rf

The isotopes ^{264,265}Rf (^{264}Rf is presently unknown) can be produced in the pxn channels of the reactions $^{18}O+^{249}Bk$ and $^{19}F+^{248}Cm$ and in the αxn channels of the reactions $^{22}Ne+^{248}Cm$ and $^{26}Mg+^{244}Pu$ (Fig. 8). For the production in pxn channels, the $^{18}O+^{249}Bk$ reaction looks more favorable due to the larger capture cross sections. The cross sections of the αxn channels in the $^{22}Ne+^{248}Cm$ reaction are slightly larger than those in the $^{26}Mg+^{244}Pu$ reaction.

The $^{22}Ne+^{248}Cm$ reaction seems to be optimal for the synthesis of the isotopes ^{264,265}Rf in the charged-particle evaporation channels [Fig. 8(c)]. The production cross sections of isotopes ^{264}Rf and ^{265}Rf are about 90 and 0.9 pb, respectively.

F. Production of $^{264–268}$Db

In Fig. 9, the calculated excitation functions of the isotopes $^{264–267}$Db (^{264,265}Db are still unknown) are shown for various fusion-evaporation reactions: in the pxn evaporation channels of the reactions $^{18}O+^{249}Cf$ (a), $^{22}Ne+^{248}Cm$ (b), $^{26}Mg+^{244}Pu$ (d), and $^{30}Si+^{238}U$ (e), and in the αxn channels of the reaction $^{22}Ne+^{249}Bk$ (c). As seen in Figs. 9(b) and 9(d), the value of the maximum of the production cross section increases with excitation energy up to the $E^*_{CN}\approx V_b+Q$, and then decreases at $E^*_{CN}\gtrsim V_b+Q$. Thus, the strong decrease of the survival probability with increasing energy under the barrier is overcompensated by the increase of the capture probability.

The reactions $^{22}Ne+^{249}Bk\rightarrow{}^{264,265}Db+\alpha 3n,\alpha 2n$ and $^{22}Ne+^{248}Cm\rightarrow{}^{266,267}Db+p3n,p2n$ are preferable for producing isotopes ^{264,265}Db [$\sigma_{\alpha 3n}(^{264}Db)=1.7$ nb, $\sigma_{\alpha 2n}(^{265}Db)=0.3$ nb] and ^{266,267}Db [$\sigma_{p3n}(^{266}Db)=33$ pb, $\sigma_{p2n}(^{267}Db)=6$ pb], respectively. Note that new ^{264}Db isotope can be produced in the $^{18}O+^{249}Bk\rightarrow{}^{264}Db+3n$ reaction with the maximum cross section of about 7 nb.

For comparison, we present the excitation functions of isotopes $^{265–268}$Db in the reactions $^{26}Mg+^{248}Cm\rightarrow{}^{269-x}Db+\alpha pxn$ and $^{26}Mg+^{249}Bk\rightarrow{}^{267-x}Db+2\alpha xn$ (Fig. 10). In the reactions $^{26}Mg+^{248}Cm$ and $^{22}Ne+^{248}Cm$, $\sigma_{\alpha pn}(^{268}Db)=0.1$ pb at $E^*_{CN}=52.5$ MeV and $\sigma_{pn}(^{268}Db)=62$ fb at $E^*_{CN}=34.4$ MeV, respectively.

G. Production of $^{266–269}$Sg

One can obtain isotopes $^{266–269}$Sg in the pxn channels of the $^{22}Ne+^{249}Bk$ reaction [Fig. 11(a)] and in the αxn channels of the reactions $^{26}Mg+^{248}Cm$ [Fig. 11(b)], $^{30}Si+^{242,244}Pu$ [Figs. 11(c) and 11(d)], and $^{36}S+^{235,238}U$ [Figs. 11(e) and 11(f)], leading to the CN ^{271,272,274}Hs*. The fusion probability in the $^{36}S+^{238}U$ reaction is much smaller ($P_{CN}\lesssim 0.14$) than those in other reactions leading to ^{274}Hs*. In the reactions $^{30}Si+^{244}Pu$ and $^{26}Mg+^{248}Cm$, P_{CN} are almost the same (about 0.6). The effective capture cross sections in the $^{26}Mg+^{248}Cm$ reaction are larger than those in the reactions $^{30}Si+^{244}Pu$ and $^{36}S+^{238}U$. Thus, in the $^{26}Mg+^{248}Cm$ reaction the production cross section is the largest in each specific channel.

Among all fusion-evaporation reactions presented in Fig. 11, the $^{26}Mg+^{248}Cm$ reaction seems to be the optimal one for producing isotopes $^{266–269}$Sg with the following cross sections: $\sigma_{\alpha 4n}(^{266}Sg)=180$ pb, $\sigma_{\alpha 3n}(^{267}Sg)=330$ pb, $\sigma_{\alpha 2n}(^{268}Sg)=40$ pb, and $\sigma_{\alpha 1n}(^{269}Sg)=0.2$ pb. Note that the $^{22}Ne+^{248}Cm$ reaction can be employed for the production of isotope ^{266}Sg [$\sigma_{4n}(^{266}Sg)=0.8$ nb] and new isotope ^{267}Sg [$\sigma_{3n}(^{267}Sg)=148$ pb] in the xn channels.

H. Production of $^{266–271}$Bh

For the production of isotopes $^{266–271}$Bh (^{268,269}Bh are still unknown), the various reaction channels are

considered: the pxn channels in the reactions ^{26}Mg + ^{248}Cm [Fig. 12(a)], ^{30}Si + ^{242,244}Pu [Figs. 12(d) and 12(e)], and ^{36}S + ^{233,235,238}U [Fig. 12(f)], and the αxn channels in the reactions ^{26}Mg + ^{249}Bk [Fig. 12(b)] and ^{27}Al + ^{248}Cm [Fig. 12(c)]. In the reactions ^{26}Mg + ^{249}Bk and ^{27}Al + ^{248}Cm leading to the same CN ^{275}Mt*, the fusion probabilities are similar, but the effective capture cross sections in the first reaction are larger. Thus, in the ^{26}Mg + ^{249}Bk reaction the production cross sections are larger, especially at $E^*_{\rm CN} \lesssim 50$ MeV due to the lower $V_b + Q$.

The ^{26}Mg + ^{249}Bk reaction is the most favorable one for the synthesis of the nuclei $^{266–270}$Bh in the charged-particle evaporation channels [$\sigma_{\alpha 5n}(^{266}\text{Bh}) = 0.6$ pb, $\sigma_{\alpha 4n}(^{267}\text{Bh}) = 15$ pb, $\sigma_{\alpha 3n}(^{268}\text{Bh}) = 120$ pb, $\sigma_{\alpha 2n}(^{269}\text{Bh}) = 55$ pb, $\sigma_{\alpha 1n}(^{270}\text{Bh}) = 0.6$ pb]. By employing the ^{22}Ne + ^{249}Bk reaction, one can also produce the isotopes $^{265–269}$Bh in the xn channels. For instance, the maximum production cross sections of ^{266}Bh and ^{267}Bh are about 50 and 200 pb, respectively.

I. Production of $^{267–274}$Hs

In the reactions ^{27}Al + ^{249}Bk [Fig. 13(a)], ^{30}Si + ^{245,248}Cm [Figs. 13(b) and 13(c)], and ^{36}S + ^{240,242,244}Pu [Figs. 13(d)–13(f)], one can produce the isotopes $^{267–274}$Hs (^{268,271,272,274}Hs are still unknown). In the ^{36}S + ^{240}Pu → ^{276}Ds* reaction, $E^*_{\rm CN} = V_b + Q$ is smaller by about 10 MeV than one in the ^{27}Al + ^{249}Bk → ^{276}Ds* reaction. Compared with the ^{27}Al + ^{249}Bk reaction, in the ^{36}S + ^{240}Pu reaction the fusion probability is a few times smaller. In this reaction the relatively lower fusion probability is overcompensated by the larger effective capture cross section at $E^*_{\rm CN} \lesssim 42$ MeV ($E_{\rm c.m.} \lesssim V_b$). As a result, the production of isotopes ^{270,271}Hs is more favorable in the ^{36}S + ^{240}Pu reaction. However, the production cross sections of isotopes ^{268,269}Hs in the ^{27}Al + ^{249}Bk reaction are larger at energies above the Coulomb barrier [$E^*_{\rm CN} \gtrsim$ 52 MeV].

In the reactions ^{30}Si + ^{248}Cm [Fig. 13(c)] and ^{36}S + ^{242}Pu [Fig. 13(e)] leading to the same CN, ^{278}Ds*, the effective capture cross sections are similar at $E^*_{\rm CN} \gtrsim 47$ MeV, but the fusion probability in the second reaction is much smaller ($P_{\rm CN} \lesssim 0.2$). Thus, the production cross sections of unknown isotope ^{271}Hs is relatively large in the ^{30}Si + ^{248}Cm reaction.

The reactions ^{30}Si + ^{245}Cm, ^{36}S + ^{240}Pu, and ^{30}Si + ^{248}Cm seem to be suitable for producing isotopes ^{268,269}Hs [$\sigma_{\alpha 3n}(^{268}\text{Hs}) = 2$ pb, $\sigma_{\alpha 2n}(^{269}\text{Hs}) = 3$ pb], ^{270}Hs [$\sigma_{\alpha 2n}(^{270}\text{Hs}) = 3$ pb], and ^{271,272}Hs [$\sigma_{\alpha 3n}(^{271}\text{Hs}) = 5$ pb, $\sigma_{\alpha 2n}(^{272}\text{Hs}) = 2$ pb], respectively. The ^{26}Mg + ^{248}Cm reaction might be optimal for producing ^{268,269}Hs in the neutron emission channels [$\sigma_{6n}(^{268}\text{Hs}) = 0.1$ pb, $\sigma_{5n}(^{269}\text{Hs}) = 6$ pb] [35]. So, the production of ^{268}Hs in the $6n$ channel is less effective than in the $\alpha 3n$ channel.

J. Production of $^{270–274}$Mt

In Fig. 14, the reactions ^{30}Si + ^{249}Bk (a) and ^{31}P + ^{248}Cm (b) lead to the same CN, ^{279}Rg*, but the former reaction has larger effective capture cross section and fusion probability, and, thus, is more suitable for producing the isotopes $^{270–274}$Mt with the following cross sections: $\sigma_{\alpha 5n}(^{270}\text{Mt}) = 0.1$ pb, $\sigma_{\alpha 4n}(^{271}\text{Mt}) = 4$ pb, $\sigma_{\alpha 3n}(^{272}\text{Mt}) =$ 22 pb, $\sigma_{\alpha 2n}(^{273}\text{Mt}) = 12$ pb, and $\sigma_{\alpha 1n}(^{274}\text{Mt}) = 0.2$ pb. In the reaction ^{26}Mg + ^{249}Bk → ^{270,271}Mt + $5n$,$4n$, the maximum production cross sections are $\sigma_{4n}(^{271}\text{Mt}) = 28$ pb and $\sigma_{5n}(^{270}\text{Mt}) = 3$ pb, respectively.

VI. SUMMARY

The production cross sections of the isotopes ^{259,260}Md, ^{260,261}No, $^{261–264}$Lr, ^{264,265}Rf, $^{264–268}$Db, $^{266–269}$Sg, $^{266–271}$Bh, $^{267–274}$Hs, and $^{270–274}$Mt in the αxn and pxn evaporation channels of the asymmetric hot fusion reactions were predicted for the first time. It was shown that the charged particle evaporation channels are suitable for producing unknown isotopes of these mentioned above with the production cross sections about 0.1 pb–1 nb. Although the production of some isotopes in xn evaporation channels is more favorable, the αxn and pxn evaporation channels allow us to obtain access to those isotopes which are unreachable in the xn channels due to the lack of proper projectile-target combination. Thus, employing the reactions suggested, one can fill a gap of unknown isotopes between the heaviest isotopes obtained in the neutron evaporation channels of the lead- and bismuth-based cold fusion and actinide-based hot fusion reactions.

ACKNOWLEDGMENTS

We are thankful to Prof. Yu.Ts. Oganessian, Prof. S. Hofmann, Prof. Y. Kim, and Prof. H. Lenske for interesting discussions and useful suggestions. This work is supported by the Rare Isotope Science Project of Institute for Basic Science funded by Ministry of Science, ICT, and Future Planning and National Research Foundation of Korea (2013M7A1A1075764). G.G.A. and N.V.A. acknowledge partial support from the Alexander von Humboldt-Stiftung (Bonn), the Russian Foundation for Basic Research (Moscow), and DFG (Bonn).

[1] Yu. Ts. Oganessian, J. Phys. G **34**, R165 (2007).

[2] Yu. Ts. Oganessian, F. S. Abdullin, P. D. Bailey, D. E. Benker, M. E. Bennett, S. N. Dmitriev, J. G. Ezold, J. H. Hamilton, R. A. Henderson, M. G. Itkis, Y. V. Lobanov, A. N. Mezentsev, K. J. Moody, S. L. Nelson, A. N. Polyakov, C. E. Porter, A. V. Ramayya, F. D. Riley, J. B. Roberto, M. A. Ryabinin, K. P. Rykaczewski, R. N. Sagaidak, D. A. Shaughnessy, I. V. Shirokovsky, M. A. Stoyer, V. G. Subbotin, R. Sudowe, A. M. Sukhov, Y. S. Tsyganov, V. K. Utyonkov, A. A. Voinov, G. K. Vostokin, and P. A. Wilk, Phys. Rev. Lett. **104**, 142502 (2010); Yu. Ts. Oganessian *et al.*, Phys. Rev. C **87**, 014302 (2013); **87**, 034605 (2013); **87**, 054621 (2013); V. K. Utyonkov, N. T. Brewer, Yu. Ts. Oganessian, K. P. Rykaczewski, F. S. Abdullin, S. N. Dmitriev, R. K. Grzywacz, M. G. Itkis, K. Miernik, A. N. Polyakov, J. B. Roberto, R. N. Sagaidak, I. V. Shirokovsky, M. V. Shumeiko, Y. S. Tsyganov, A. A. Voinov, V. G. Subbotin, A.

M. Sukhov, A. V. Sabelnikov, G. K. Vostokin, J. H. Hamilton, M. A. Stoyer, and S. Y. Strauss, *ibid.* **92**, 034609 (2015).
[3] Yu. Ts. Oganessian and V. K. Utyonkov, Nucl. Phys. A **944**, 62 (2015).
[4] R. Eichler *et al.*, Nature (London) **447**, 72 (2007).
[5] S. Hofmann *et al.*, Eur. Phys. J. A **32**, 251 (2007).
[6] L. Stavsetra, K. E. Gregorich, J. Dvorak, P. A. Ellison, I. Dragojevic, M. A. Garcia, and H. Nitsche, Phys. Rev. Lett. **103**, 132502 (2009).
[7] C. E. Düllmann, M. Schadel, A. Yakushev, A. Turler, K. Eberhardt, J. V. Kratz, D. Ackermann, L. L. Andersson, M. Block, W. Bruchle, J. Dvorak, H. G. Essel, P. A. Ellison, J. Even, J. M. Gates, A. Gorshkov, R. Graeger, K. E. Gregorich, W. Hartmann, R. D. Herzberg, F. P. Hessberger, D. Hild, A. Hubner, E. Jager, J. Khuyagbaatar, B. Kindler, J. Krier, N. Kurz, S. Lahiri, D. Liebe, B. Lommel, M. Maiti, H. Nitsche, J. P. Omtvedt, E. Parr, D. Rudolph, J. Runke, B. Schausten, E. Schimpf, A. Semchenkov, J. Steiner, P. Thorle-Pospiech, J. Uusitalo, M. Wegrzecki, and N. Wiehl, Phys. Rev. Lett. **104**, 252701 (2010).
[8] J. M. Gates, C. E. Dullmann, M. Schadel, A. Yakushev, A. Turler, K. Eberhardt, J. V. Kratz, D. Ackermann, L. L. Andersson, M. Block, W. Bruchle, J. Dvorak, H. G. Essel, P. A. Ellison, J. Even, U. Forsberg, J. Gellanki, A. Gorshkov, R. Graeger, K. E. Gregorich, W. Hartmann, R. D. Herzberg, F. P. Hessberger, D. Hild, A. Hubner, E. Jager, J. Khuyagbaatar, B. Kindler, J. Krier, N. Kurz, S. Lahiri, D. Liebe, B. Lommel, M. Maiti, H. Nitsche, J. P. Omtvedt, E. Parr, D. Rudolph, J. Runke, H. Schaffner, B. Schausten, E. Schimpf, A. Semchenkov, J. Steiner, P. Thorle-Pospiech, J. Uusitalo, M. Wegrzecki, and N. Wiehl, Phys. Rev. C **83**, 054618 (2011).
[9] S. Hofmann *et al.*, Eur. Phys. J. A **48**, 62 (2012).
[10] J. M. Khuyagbaatar *et al.*, Phys. Rev. Lett. **112**, 172501 (2014).
[11] S. Hofmann *et al.*, Eur. Phys. J. A **52**, 180 (2016).
[12] S. Hofmann and G. Münzenberg, Rev. Mod. Phys. **72**, 733 (2000).
[13] K. Morita *et al.*, Eur. Phys. J. A **21**, 257 (2004); J. Phys. Soc. Jpn. **73**, 2593 (2004); **76**, 043201 (2007).
[14] J. Peter *et al.*, Nucl. Phys. A **734**, 192 (2004).
[15] S. Hofmann, Lect. Notes Phys. **764**, 203 (2009); Radiochim. Acta **99**, 405 (2011).
[16] V. V. Volkov, Phys. Rep. **44**, 93 (1978); *Nuclear Reactions of Deep Inelastic Transfers* (Energoizdat, Moscow, 1982).
[17] W. U. Schröder and J. R. Huizenga, in *Treatise on Heavy-Ion Science*, edited by D. A. Bromley (Plenum Press, New York, 1984), Vol. 2, p. 115.
[18] R. T. de Souza, J. R. Huizenga, and W. U. Schröder, Phys. Rev. C **37**, 1901 (1988); R. T. de Souza, W. U. Schroder, J. R. Huizenga, J. Toke, S. S. Datta, and J. L. Wile, *ibid.* **39**, 114 (1989).
[19] V. V. Volkov, in *Treatise on Heavy-Ion Science*, edited by D. A. Bromley (Plenum Press, New York, 1989), Vol. 8, p. 255.
[20] J. Randrup, Nucl. Phys. A **307**, 319 (1978); **327**, 490 (1979).
[21] G. G. Adamian, A. K. Nasirov, N. V. Antonenko, and R. V. Jolos, Phys. Part. Nucl. **25**, 583 (1994).
[22] G. G. Adamian, N. V. Antonenko, and A. S. Zubov, Phys. Rev. C **71**, 034603 (2005).
[23] Yu. Ts. Oganessian (private communication).
[24] N. V. Antonenko, E. A. Cherepanov, A. K. Nasirov, V. P. Permjakov, and V. V. Volkov, Phys. Lett. B **319**, 425 (1993); Phys. Rev. C **51**, 2635 (1995).
[25] G. G. Adamian, N. V. Antonenko, W. Scheid, and V. V. Volkov, Nucl. Phys. A **633**, 409 (1998); Nuovo Cimento A **110**, 1143 (1997).
[26] G. G. Adamian, N. V. Antonenko, and W. Scheid, Nucl. Phys. A **678**, 24 (2000).
[27] G. G. Giardina, S. Hofmann, A. I. Muminov, and A. K. Nasirov, Eur. Phys. J. A **8**, 205 (2000); G. G. Giardina, F. Hanappe, A. I. Muminov, A. K. Nasirov, and L. Stuttgé, Nucl. Phys. A **671**, 165 (2000); A. K. Nasirov *et al.*, *ibid.* **759**, 342 (2005); H. Q. Hang, C. L. Zhang, C. J. Lin, Z. H. Liu, F. Yang, A. K. Nasirov, G. Mandaglio, M. Manganaro, and G. Giardina, Phys. Rev. C **81**, 034611 (2010); A. K. Nasirov, G. Mandaglio, G. G. Giardina, A. Sobiczewski, and A. I. Muminov, *ibid.* **84**, 044612 (2011).
[28] Z. H. Liu and J. D. Bao, Phys. Rev. C **74**, 057602 (2006).
[29] N. Wang, J. Tian, and W. Scheid, Phys. Rev. C **84**, 061601(R) (2011).
[30] N. Wang, E. G. Zhao, W. Scheid, and S. G. Zhou, Phys. Rev. C **85**, 041601(R) (2012); N. Wang, E. G. Zhao, and W. Scheid, *ibid.* **89**, 037601 (2014).
[31] L. Zhu, Z. Q. Feng, C. Li, and F. S. Zhang, Phys. Rev. C **90**, 014612 (2014); Z. Q. Feng, G. M. Jin, J. Q. Li, and W. Scheid, *ibid.* **76**, 044606 (2007).
[32] A. S. Zubov, G. G. Adamian, N. V. Antonenko, S. P. Ivanova, and W. Scheid, Phys. Rev. C **68**, 014616 (2003).
[33] G. G. Adamian, N. V. Antonenko, W. Scheid, and A. S. Zubov, Phys. Rev. C **78**, 044605 (2008).
[34] G. G. Adamian, N. V. Antonenko, and W. Scheid, *Clustering Effects within the Dinuclear Model*, Lecture Notes in Physics Vol. 848, edited by Christian Beck (Springer, Heidelberg, 2012), p. 165.
[35] J. Hong, G. G. Adamian, and N. V. Antonenko, Phys. Rev. C **92**, 014617 (2015).
[36] V. S. Barashenkov and V. D. Toneev, *High Energy Interaction of Particles and Nuclei with Atomic Nuclei* (Atomizdat, Moscow, 1972).
[37] R. Vandenbosch and J. R. Huizenga, *Nuclear Fission* (Academic Press, New York, 1973).
[38] A. Ignatyuk, *Statistical Properties of Excited Atomic Nuclei* (Energoatomizdat, Moscow, 1983).
[39] E. A. Cherepanov, A. S. Iljinov, and M. V. Mebel, J. Phys. G **9**, 931 (1983).
[40] K. H. Schmidt and W. Morawek, Rep. Prog. Phys. **54**, 949 (1991).
[41] A. S. Iljinov *et al.*, Nucl. Phys. A **543**, 517 (1992).
[42] A. S. Zubov, G. G. Adamian, N. V. Antonenko, S. P. Ivanova, and W. Scheid, Phys. Rev. C **65**, 024308 (2002).
[43] S. G. Mashnik, A. J. Sierk, and K. K. Gudima, arXiv:nucl-th/0208048.
[44] A. J. Sierk, Phys. Rev. C **33**, 2039 (1986).
[45] N. Shinohara, S. Usuda, S. Ichikawa, T. Suzuki, M. Magara, H. Okashita, H. Yoshikawa, T. Horiguchi, Y. Iwata, S. Shibata, and I. Fujiwara, Phys. Rev. C **34**, 909 (1986).
[46] V. A. Druin, Yu. V. Lobanov, R. N. Sagaydak, and E. A. Cherepanov, *Intern. School-Seminar, Alushta* (JINR, Dubna, 1983), p. 233.
[47] M. Murakami, S. Goto, H. Murayama, T. Kojima, H. Kudo, D. Kaji, K. Morimoto, H. Haba, Y. Kudou, T. Sumita, R. Sakai, A. Yoneda, K. Morita, Y. Kasamatsu, H. Kikunaga, and T. K. Sato, Phys. Rev. C **88**, 024618 (2013).

[48] A. Ghiorso, M. Nurmia, K. Eskola, J. Harris, and P. Eskola, Phys. Rev. Lett. **24**, 1498 (1970).
[49] G. G. Adamian *et al.*, Int. J. Mod. Phys. E **05**, 191 (1996).
[50] P. Möller, J. R. Nix, W. D. Myers, and W. J. Swiatecki, At. Data Nucl. Data Tables **59**, 185 (1995).
[51] T. Sikkeland, J. Maly, and D. F. Lebeck, Phys. Rev. **169**, 1000 (1968).
[52] M. Nurmia, T. Sikkeland, R. Silva, and A. Ghiorso, Phys. Lett. B **26**, 78 (1967).
[53] R. N. Sagaidak *et al.*, J. Phys. G **24**, 611 (1998).
[54] K. Eskola, P. Eskola, M. Nurmia, and A. Ghiorso, Phys. Rev. C **4**, 632 (1971).
[55] A. V. Yeremin, Phys. Part. Nuclei **38**, 492 (2007).
[56] J. M. Nitschke *et al.*, Nucl. Phys. A **352**, 138 (1981); L. P. Somerville, M. J. Nurmia, J. M. Nitschke, A. Ghiorso, E. K. Hulet, and R. W. Lougheed, Phys. Rev. C **31**, 1801 (1985).
[57] Y. A. Lazarev, Y. V. Lobanov, Yu. Ts. Oganessian, V. K. Utyonkov, F. S. Abdullin, A. N. Polyakov, J. Rigol, I. V. Shirokovsky, Y. S. Tsyganov, S. Iliev, V. G. Subbotin, A. M. Sukhov, G. V. Buklanov, A. N. Mezentsev, K. Subotic, K. J. Moody, N. J. Stoyer, J. F. Wild, and R. W. Lougheed, Phys. Rev. C **62**, 064307 (2000).
[58] M. R. Lane, K. E. Gregorich, D. M. Lee, M. F. Mohar, M. Hsu, C. D. Kacher, B. Kadkhodayan, M. P. Neu, N. J. Stoyer, E. R. Sylwester, J. C. Yang, and D. C. Hoffman, Phys. Rev. C **53**, 2893 (1996).
[59] P. A. Wilk, K. E. Gregorich, A. Turler, C. A. Laue, R. Eichler, V. Ninov, J. L. Adams, U. W. Kirbach, M. R. Lane, D. M. Lee, J. B. Patin, D. A. Shaughnessy, D. A. Strellis, H. Nitsche, and D. C. Hoffman, Phys. Rev. Lett. **85**, 2697 (2000).
[60] H. Haba, M. Huang, D. Kaji, J. Kanaya, Y. Kudou, K. Morimoto, K. Morita, M. Murakami, K. Ozeki, R. Sakai, T. Sumita, Y. Wakabayashi, A. Yoneda, Y. Kasamatsu, Y. Kikutani, Y. Komori, K. Nakamura, A. Shinohara, H. Kikunaga, H. Kudo, K. Nishio, A. Toyoshima, and K. Tsukada, Phys. Rev. C **89**, 024618 (2014).
[61] J. V. Kratz, M. K. Gober, H. P. Zimmermann, M. Schadel, W. Bruchle, E. Schimpf, K. E. Gregorich, A. Turler, N. J. Hannink, K. R. Czerwinski, B. Kadkhodayan, D. M. Lee, M. J. Nurmia, D. C. Hoffman, H. Gaggeler, D. Jost, J. Kovacs, U. W. Scherer, and A. Weber, Phys. Rev. C **45**, 1064 (1992); J. V. Kratz *et al.*, Radiochim. Acta **91**, 59 (2003).
[62] Z. G. Gan *et al.*, Eur. Phys. J. A **10**, 21 (2001).
[63] M. R. Lane, K. E. Gregorich, D. M. Lee, B. Wierczinski, C. A. McGrath, M. B. Hendricks, D. A. Shaughnessy, D. A. Strellis, E. R. Sylwester, P. A. Wilk, and D. C. Hoffman, Phys. Rev. C **58**, 3413 (1998).
[64] A. N. Andreyev *et al.*, Z. Phys. A **344**, 225 (1992).
[65] A. Ghiorso, J. M. Nitschke, J. R. Alonso, C. T. Alonso, A. Nurmia, G. T. Seaborg, E. K. Hulet, and R. W. Lougheed, Phys. Rev. Lett. **33**, 1490 (1974).
[66] K. Nishio *et al.*, Eur. Phys. J. A **29**, 281 (2006).
[67] G. N. Akapiev *et al.*, Atom. Ener. **21**, 243 (1966); K. Nishio *et al.*, JAERI Rev. 2004-027 (JAERI, Tokai-mura, 2004), p. 39; R. N. Sagaidak, Eur. Phys. J. D **45**, 59 (2007).
[68] Y. Nagame *et al.*, J. Nucl. Radiochem. Sci. **3**, 85 (2002).
[69] Y. A. Lazarev, Y. V. Lobanov, Yu. Ts. Oganessian, V. K. Utyonkov, F. S. Abdullin, G. V. Buklanov, B. N. Gikal, S. Iliev, A. N. Mezentsev, A. N. Polyakov, I. M. Sedykh, I. V. Shirokovsky, V. G. Subbotin, A. M. Sukhov, Y. S. Tsyganov, V. E. Zhuchko, R. W. Lougheed, K. J. Moody, J. F. Wild, E. K. Hulet, and J. H. McQuaid, Phys. Rev. Lett. **73**, 624 (1994); Ch. E. Düllmann and A. Türler, Phys. Rev. C **77**, 064320 (2008); H. Haba, D. Kaji, Y. Kudou, K. Morimoto, K. Morita, K. Ozeki, R. Sakai, T. Sumita, A. Yoneda, Y. Kasamatsu, Y. Komori, A. Shinohara, H. Kikunaga, H. Kudo, K. Nishio, K. Ooe, N. Sato, and K. Tsukada, *ibid.* **85**, 024611 (2012).